Predicting air quality: Improvements through advanced methods to integrate models and measurements

Gregory R. Carmichael [a,*], Adrian Sandu [b], Tianfeng Chai [a], Dacian N. Daescu [c], Emil M. Constantinescu [b], Youhua Tang [a]

[a] *The University of Iowa, CGRER, Iowa City, IA 52242, USA*
[b] *Virginia Polytechnic University, Department of Computer Science, Blacksburg, VA 24061, USA*
[c] *Portland State University, Department of Mathematics and Statistics, Portland, OR 97207, USA*

Abstract

Air quality prediction plays an important role in the management of our environment. Computational power and efficiencies have advanced to the point where chemical transport models can predict pollution in an urban air shed with spatial resolution less than a kilometer, and cover the globe with a horizontal resolution of less than 50 km. Predicting air quality remains a challenge due to the complexity of the governing processes and the strong coupling across scales. While air quality prediction is closely aligned with weather prediction, there are important differences, including the role of pollution emissions and their associated large uncertainties. Improvements in air quality prediction require a close integration of observations. As more atmospheric chemical observations become available chemical data assimilation is expected to play an essential role in air quality forecasting. In this paper advances in air quality forecasting are discussed with an emphasis on data assimilation. Applications of the four-dimensional variational method (4D-Var) and the ensemble Kalman filter (EnKF) approach are presented and the computation challenges are discussed.
© 2007 Elsevier Inc. All rights reserved.

Keywords: Air quality forecasting; Data assimilation; Ozone pollution

1. Introduction

Predicting air quality is of growing importance to society. The chemical composition of the atmosphere has been (and is being) significantly perturbed by emissions of trace gases and aerosols associated with a variety of anthropogenic activities. This changing of the chemical composition of the atmosphere has important implications for urban, regional and global air quality, and for climate change. In the US alone more than 450 counties with nearly 160 million inhabitants, are currently in some degree of non-attainment with respect

to the 8-h National Ambient Air Quality Standard (NAAQS) for ground-level ozone (80 ppbv). Because air quality problems relate to immediate human welfare, their study has traditionally been driven by the need for information to guide policy.

Chemical transport models (CTMs) have become an essential tool for providing science-based input into best alternatives for reducing urban pollution levels, for designing cost-effective emission control strategies, for the interpretation of observational data, and for assessments into how we have altered the chemistry of the global environment. The use of CTMs to produce air quality forecasts has become a new application area, providing important information to the public, decision makers and researchers. Currently hundreds of cities world-wide are providing real time air quality forecasts. In addition, national weather services throughout the world are broadening their traditional role of mesoscale weather prediction to also include prediction of other environmental phenomena (e.g. plumes from biomass burning, volcanic eruptions dust storms, and urban air pollution) that could potentially affect the health and welfare of their inhabitants. For example, the US National Weather Service (NWS) has recently started to provide mesoscale numerical model forecast guidance for short-term air quality predictions, beginning with next-day ozone (O_3) forecasts for the northeastern, and plans to expand this air quality capability over the next ten years to include the entire US, to lengthen the forecast period to 3-days, and to add fine particulate matter (PM2.5) to the forecasts.

The use of CTMs in chemical weather (in this paper we will use the terms chemical weather and air quality interchangeably) forecasting applications in support of field experiments is another important application, which began with stratospheric experiments in the 1990s [82,29,108]. CTMs have now become an integral part of large field experiments; see [79] and references therein for an excellent summary of CTMs used in chemical weather forecasting activities associated with several recent field experiments.

Over the last decade our ability to predict air quality has improved due to significant advancements in our ability to measure and model atmospheric chemistry, transport and removal processes. We are now able to measure at surface sites and on mobile platforms (such as vans, ships and aircraft), with fast response times and wide dynamic range, many of the important primary and secondary atmospheric trace gases and aerosols (e.g. carbon monoxide, ozone, sulfur dioxide, black carbon, etc.), and many of the critical photochemical oxidizing agents (such as the OH and HO_2 radicals). Not only is our ability to characterize a fixed atmospheric point in space and time expanding, but the spatial coverage is also expanding through growing capabilities to measure atmospheric constituents remotely using sensors mounted at the surface and on satellites. From the modeling perspective, CTMs have advanced to the point where they now follow scores of chemical species, interacting through chemical mechanisms involving hundreds of chemical reactions. In addition, the transport aspects of CTMs are now run in close interaction with dynamic meteorological models. Computational power and efficiencies have advanced to the point where CTMs can simulate pollution distributions in an urban air shed with spatial resolution of less than a kilometer, and can cover the entire globe with horizontal grid spacing of less than 50–100 km.

While significant advances in CTMs have taken place, predicting air quality remains a challenging problem due to the complex processes occurring at widely different scales and by their strong coupling across scales. Fig. 1 illustrates some of the complexities in air quality predictions. Models have been developed for the simulation of these processes at each scale (right). These models have to balance fidelity (i.e. the accuracy of the description of the physical and chemical processes) and computational cost. Very detailed zero-dimensional (''box'') models incorporate high fidelity descriptions of the chemistry, aerosol and atmospheric dynamics, and thermodynamics. For larger areas, models incorporate more processes and employ more grid points; but for computational feasibility the spatial and temporal resolution is decreased, and the fidelity of each component is reduced.

Air quality predictions have large uncertainties associated with: incomplete and/or inaccurate emissions information; lack of key measurements to impose initial and boundary conditions; missing science elements; and poorly parameterized processes. Improvements in the predictive capabilities of CTMs require them to be better constrained through the use of observational data. Borrowing lessons learned from the evolution of numerical weather prediction (NWP) models, improving air quality predictions through the assimilation of chemical data holds significant promise. In this paper we present current activities focused on improving the prediction capabilities of CTMs through the use of advanced methods. Specifically we focus on techniques to integrate models with measurements.
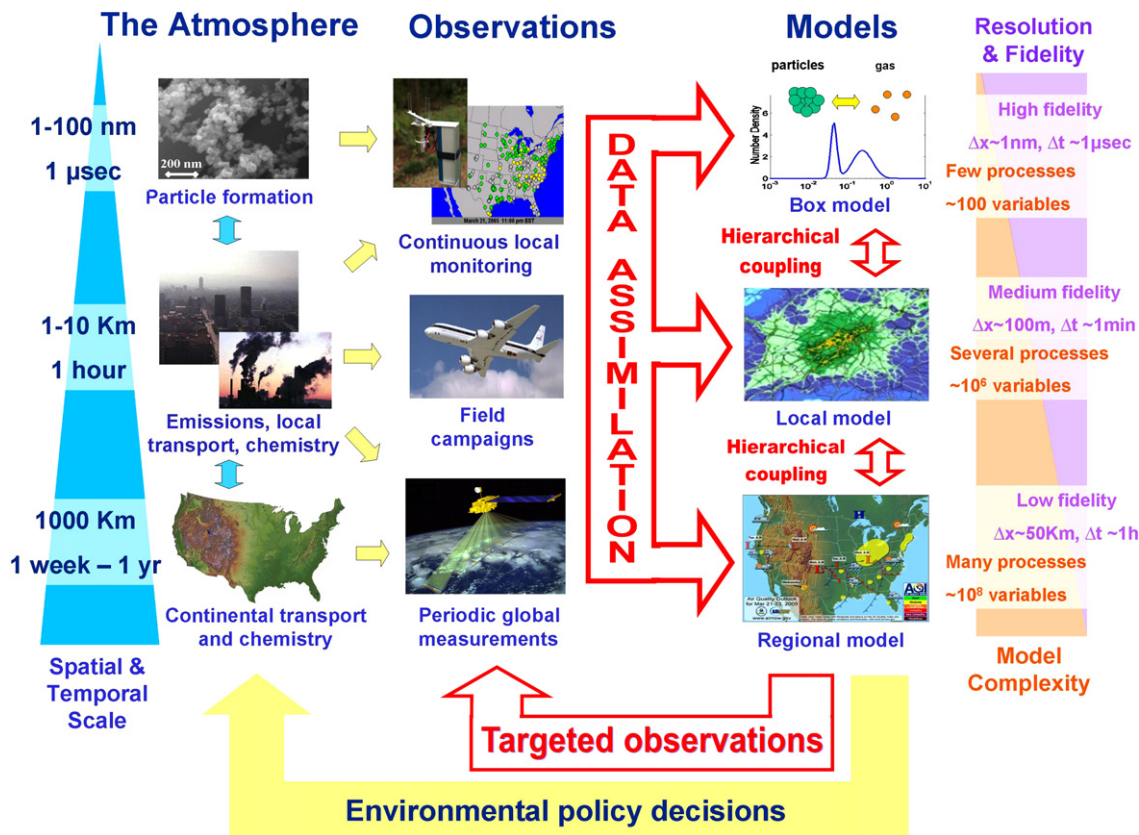
Fig. 1. Information feedback loops between models and observations as they relate to predicting air quality. Complex CTMs incorporate chemical, aerosol, radiation modules, and use information from meteorological simulations (e.g. wind and temperature fields, turbulent diffusion parameterizations) and from emission inventories to produce chemical weather forecast. Yellow arrows represent the data flow for predictions using the first principles. Another source of information for concentrations of pollutants in the atmosphere is the observations. Data assimilation combines these two sources of information to produce an optimal analysis state of the atmosphere, consistent with both the physical/chemical laws of evolution through the model (first principles) and with reality through measurement information. Pink arrows illustrate the data flow for dynamic feedback and control loop from measurements/data assimilation to simulation. Targeted observations locate the observations in space and time such that the uncertainty in predictions is minimized.

2. Mathematical framework

An atmospheric CTM solves for the mass balance equations for concentrations y_i of tracer species $1 \leqslant i \leqslant n$. The tracer species can be in gas, liquid, or particulate phases, and their concentrations are continuously changed by multiple physical and chemical processes

$$
\begin{aligned}
&\frac{\partial y_i}{\partial t} = -\vec{u} \cdot \nabla y_i + \frac{1}{\rho} \nabla \cdot (\rho K \nabla y_i) + \frac{1}{\rho} f_i(\rho y) + E_i, \quad 1 \leqslant i \leqslant n, \ t^0 \leqslant t \leqslant t^F \\
&y_i(t^0, x) = y_i^0(x), \\
&y_i(t, x) = y_i^{IN}(t, x) \quad \text{on } \Gamma^{IN}, \\
&K_{nn} \frac{\partial y_i}{\partial n} = 0 \quad \text{on } \Gamma^{OUT}, \\
&K_{nn} \frac{\partial y_i}{\partial n} = V_i^{DEP} y_i - Q_i \quad \text{on } \Gamma^{GROUND}
\end{aligned}
\tag{1}
$$

Here $\vec{u}$ represents the wind velocity vector, K is the turbulent diffusion tensor, and ρ is the air density. These variables are typically prescribed from simulations with a numerical weather prediction model. The concen-

trations y_i are expressed as a mole fraction (e.g. the number of molecules of tracer per 1 billion molecules of air); the absolute concentration of tracer i is ρy_i (molecules/cm^3). f_i is the rate of transformations of species i and depends on all other concentrations at the same spatial location. Such local transformations are determined by gas and liquid phase chemical kinetics, by inter-phase mass transfer, by aerosol dynamic processes (coagulation and growth), by thermodynamic processes, etc. The elevated emissions of species i are E_i and the ground level emissions are Q_i. The deposition velocity is V_i^{DEP}. The model has prescribed initial conditions y_i^0 and is subject to Dirichlet boundary conditions at the inflow (lateral and top) boundary Γ^{IN}, to no diffusive flow condition at the outflow (lateral and top) boundary Γ^{OUT}, and to Neumann boundary conditions at the ground level boundary Γ^{GROUND}.

The numerical solution to (1) can be represented by

$$y^k = M(t^{k-1}, y^{k-1}, p), \quad y^0 = y(t^0), \qquad k = 1, 2, \ldots \tag{2}$$

In (2), the solution y^k is the discrete state vector containing the dependent variables at time t^k (e.g. concentrations of chemical species), p is the vector of model parameters (e.g. the emission rates, deposition velocities, boundary fluxes), and M is the discrete model solution operator. Computational issues will be discussed later in Section 7.

3. Air quality forecasting

Air quality forecasts built upon CTM predictions (in contrast to other techniques such as statistical methods) contain components related to emissions, transport, transformation and removal processes as described by (1). Since the four-dimensional distribution of pollutants in the atmosphere is heavily influenced by the prevailing meteorological conditions, air quality models are closely aligned with weather prediction. Air quality forecast models are driven by meteorological models (global and/or mesoscale), and this coupling is done in off-line or on-line modes, referring to whether the air quality constituents are calculated within the meteorological model itself (on-line, e.g. WRF/Chem [58]) or calculated in a separate model, which accepts the meteorological fields as inputs (off-line).

Air quality forecasting differs in important ways from the problem of weather forecasting. One important difference is that weather prediction is typically focused on severe, adverse weather conditions (e.g. storms), while the meteorology of adverse air quality conditions frequently is associated with benign weather. Boundary-layer structure and wind direction are perhaps the two most poorly determined meteorological variables for air quality prediction. Meteorological observations are critical to effectively predict air quality, yet meteorological observing systems are typically designed to support prediction of severe weather and not the subtleties of adverse air quality. Research needs associated with the meteorological elements of air quality prediction have recently been assessed [36].

Air quality predictions also differ from weather forecasting due to the additional processes associated with emissions, chemical transformations, and removal. Because many important pollutants (e.g. ozone and fine particulate sulfate) are secondary in nature (i.e. formed via chemical reactions in the atmosphere), air quality models must include a rich description of the photochemical oxidant cycle. A schematic of the chemistry of the atmosphere represented in air quality predictions is shown in Fig. 2. A long standing challenge in air quality prediction is to select a chemical mechanism that captures the proper balance between chemical complexity and computational efficiency. Explicit mechanisms such as the Leeds Master Chemical Mechanism [71] treat large numbers of species and reactions, but such explicit treatments are computationally expensive. The development of reduced mechanisms remains an active area of laboratory and computational research [23,125,89]. Contemporary air quality models typically include hundreds of chemical variables (including gas phase constituents and aerosol species distributed by composition and size). The resulting system of equations is stiff and highly coupled, which greatly adds to the computational burden of air quality forecasting.

It is also important to note that the chemical and removal processes are highly coupled to meteorology variables (e.g. temperature and water vapor), as are many of the emission terms; directly in the case of wind blown soils whose emission rates correlate with surface winds and evaporative emissions that correlate with temperature, and indirectly in the case of those associated with heating and cooling demand that responds to ambient temperatures.
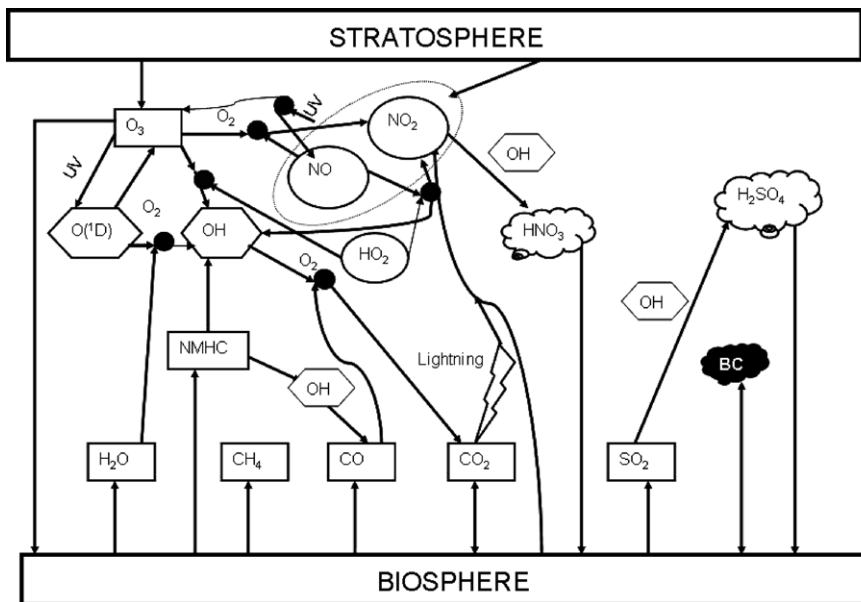
Fig. 2. Schematic illustration of some of the important chemical processes, key species, and their couplings that are included in chemical weather forecasting models.

The capabilities of current CTMs used in air quality forecasting are illustrated using results from the STEM model application during the NASA TRACE-P (Tropospheric Atmospheric Chemistry Pacific Experiment [70]) study [22]. The model results are compared to the 5-min merged data set for observations taken on-board the DC-8 aircraft. The model was sampled every five minutes along each flight-track for the period when the aircrafts were operating in the western Pacific (4 March to 2 April 2001). Model results were interpolated to the aircraft location and time (using tri-linear and linear interpolation). The correlation coefficients for a variety of meteorological and chemical variables are plotted in Fig. 3. As we discuss these predictions it is important to keep in mind the issue of how to judge these results. What are (or should be) our expectations of the capabilities to predict ambient levels of trace species in a given region? It can be argued that our capability to predict ambient trace species should be less than that for the meteorological parameters, given that the trace gas species distributions depend on the meteorological fields themselves and also on the emission estimates,
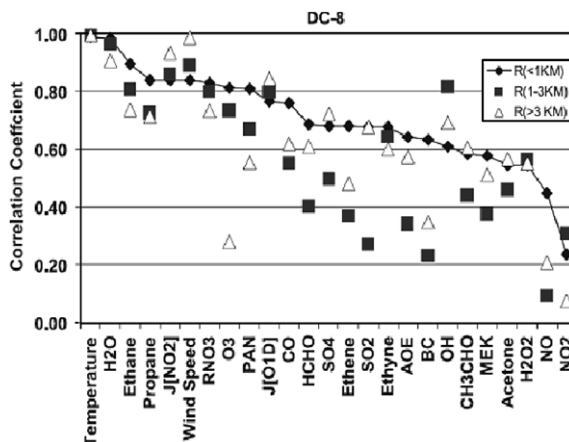

Fig. 3. Correlation coefficients between observed and modeled meteorological and chemical species for the <1 km, 1–3 km, and >3 km altitude bins using the DC-8 aircraft data.

which themselves are highly uncertain. Further complicating our ability to predict trace species is the nonlinearity and species interdependencies introduced by the photochemical oxidant cycle. As shown in Fig. 3 the meteorological parameters are modeled most accurately. The better skill in predicting these meteorological variables reflects the large amount of observational data ingested into the analysis of the large-scale meteorological fields. However, even with this large amount of assimilated information, the differences between the mean observed and modeled water vapor concentrations away from the surface remain significant (i.e. 30–40% above 3 km). The correlation coefficients for the trace species are lower than those for the meteorological parameters.

In general the predictive skill for the chemical species decreases with distance above the surface, reflecting the increased uncertainty associated with vertical transport processes. An inter-comparison of four global scale and three regional scale chemical transport models using TRACE-P CO observations found substantial differences in spatial distributions and column amounts due to meteorological processes [74]. Model differences in treatment of planetary boundary layer dynamics, vertical convection and lifting in frontal zones, were found to result in differences in modeled column amounts along specific flight paths of a factor of 2.

Currently most air quality forecasts are based on limited area models in order to achieve the requisite temporal and spatial representation. For such applications an additional source of uncertainty is the boundary conditions. One current approach to improving air quality forecasts is to drive the limited area forecasts with boundary conditions (BCs) provided by global chemical weather forecasts. The sensitivity of the predictions of a limited area model to various treatments of the boundary conditions is available in [121], where it is shown that the temporal and spatial variability introduced via the global models generally improved model predictions. However the global CTM predictions are also a source of uncertainty. For example, ozone predictions using BCs from three different global model were shown to vary by more than 20%. Reducing the uncertainty in the BCs provided by global CTMs is a critical step toward improving air quality predictions.

4. Sensitivity and uncertainty analysis

An essential element to advance the predictive skill of air quality forecasts is to improve the forward model (i.e. the underlying CTM). Sensitivity analysis of the CTM can help: (i) identify sensitive regions where uncertainty in the model parameters can lead to large errors in the predictions; (ii) explore important feedback processes; and (iii) guide improvements in the prediction skills in air quality forecasts. Here we discuss some current approaches to sensitivity analysis.

Sensitivity analysis is a formal methodology to assess the rate of change of the solution of the model when small perturbations are made to model parameters (including initial values, boundary conditions and emissions) [20]. The rate of change of the solution with respect to the ith model parameter (i.e. the sensitivity of the solution with respect to the ith parameter) is denoted by

$$S_i(t) = \frac{\partial y(t)}{\partial p_i}, \quad S_i^k = \frac{\partial y^k}{\partial p_i} \tag{3}$$

When the model solution and model parameters have different magnitudes, or different units, it is advantageous to consider scaled sensitivity coefficients

$$\widehat{S}_i(t) = \frac{\partial y(t)}{\partial p_i} \cdot \frac{p_i}{y(t)} \tag{4}$$

4.1. Direct sensitivity analysis: a source-oriented approach

The sensitivities of the model solution evolve in time according to the linearized model dynamics

$$S_i^k = \frac{\partial M}{\partial y}(y^{k-1}, p)S_i^{k-1} + \frac{\partial M}{\partial p_i}(y^{k-1}, p), \quad S_i^0 = \frac{\partial y^0}{\partial p_i}, \qquad 1 \leqslant k \leqslant F \tag{5}$$

Here M is the operator that advances y, i.e. $y^k = M(y^{k-1}, p)$, and F is the number of time steps. The direct sensitivity analysis approach solves for the model together with the sensitivity equation, and advances both

forward in time. Note that there are as many sensitivity equations to solve as there are parameters, $1 \leqslant i \leqslant m$. Computational savings are possible by reusing the same linear algebra factorizations in the forward model and in all the sensitivity equations (the direct decoupled method for sensitivity analysis) [45],

$$S_i^k = \frac{\partial M}{\partial y}(y^{k-1}) \cdot S_i^{k-1}, \quad S_i^0 = \frac{\partial y^0}{\partial y_i^0} = e_i, \qquad 0 \leqslant k \leqslant F \tag{6}$$

where e_i is a vector with all entries equal to zero, except for entry I, which is equal to 1. The source-oriented sensitivity analysis approach is illustrated in Fig. 4(a), where an initial perturbation at a source location i is propagated throughout the modeling domain at future times.

Consequently, the direct sensitivity analysis approach is effective when the changes in all concentration levels across all grid points with respect to changes in few model parameters are needed. Direct sensitivity analysis is effective to compute the effect of changing few sources onto the entire concentration field.

4.2. Adjoint sensitivity analysis: a receptor-oriented approach

In many instances one is interested to assess the sensitivities of a cost function defined on the concentration field at the final time

$$\text{Given} \quad \Psi(y^F(p)) \in \mathfrak{R} \quad \text{evaluate} \quad \nabla_p \Psi = \left(\frac{\partial \Psi}{\partial p}\right)^T = \begin{bmatrix} \frac{\partial \Psi}{\partial p_1} \\ \vdots \\ \frac{\partial \Psi}{\partial p_m} \end{bmatrix} \in \mathfrak{R}^m \tag{7}$$

The simplest example of a cost function is the concentration of a given species (e.g. ozone) at a given "receptor" location at the end of the simulation interval: $\Psi(y^F) = y_j(t^F)$. This is illustrated in Fig. 4(b): the value of the cost function at the receptor time and location is influenced by changes in concentrations, emissions, etc. at earlier times throughout the modeling domain.

Formally if we denote by λ^k the adjoint variables and impose that they satisfy the following adjoint equations:

$$
\begin{aligned}
\lambda^F &= \left(\frac{\partial \Psi(y^F)}{\partial y^k}\right)^T, \\
\lambda^{k-1} &= \left(\frac{\partial y^k}{\partial y^{k-1}}\right)^T \lambda^k = \left(\frac{\partial M(p, y^{k-1})}{\partial y}\right)^T \lambda^k, \quad 1 \leqslant k \leqslant F
\end{aligned}
\tag{8}
$$

then the adjoint variables are the gradients of the cost function with respect to changes in the state at earlier times
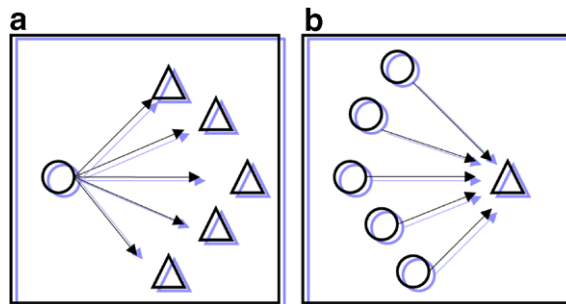

Fig. 4. (a) Direct sensitivity analysis is a source-oriented approach: the perturbation from one source is evolved and is followed by many receptors. (b) Adjoint sensitivity analysis is a receptor-oriented approach: perturbations from many sources are evolved simultaneously, and their effect is measured at one receptor.

$$\lambda^k = \left(\frac{\partial \Psi(y^{\mathrm{F}})}{\partial y^k}\right)^{\mathrm{T}} = \nabla_{y^k} \Psi(y^{\mathrm{F}}) \tag{9}$$

For the general situation the sensitivity of the cost function with respect to model parameters is obtained by a single integration of the adjoint model backward in time, via the relation

$$\nabla_{p_i} \Psi = \left(\frac{\partial y^0}{\partial p_i}\right)^{\mathrm{T}} + \sum_{k=1}^{\mathrm{F}} \left(\frac{\partial M}{\partial p_i}(p, y^{k-1})\right)^{\mathrm{T}} \lambda^k, \quad 1 \leqslant i \leqslant m \tag{10}$$

Note that the same adjoint variables are used to obtain the sensitivities with respect to all parameters; thus a single backward integration of the adjoint model is sufficient. Mathematical foundations of the adjoint sensitivity for nonlinear dynamical systems and various classes of response functionals are presented in [18–20,92].

4.3. Continuous adjoint models vs. discrete adjoint models

As explained above, the adjoint model (8) was obtained from the mass balance equations (1) by first discretizing them (2), then taking the adjoint of the tangent linear form of the discretization (applying a linearization and the transposed chain rule). For this reason the model (8) is called the "discrete adjoint model" and is obtained by a "discretize then linearize and transpose" approach. The adjoint variables λ^k of (8) represent the sensitivities of the discrete cost function (7) with respect to the numerical solution y^k.

In a more general functional-analytic framework [114] the sensitivities of a cost functional defined on the solution of the continuous mass balance equations (1) can be analyzed. It can be shown that the sensitivities of the cost functional with respect to the continuous solution (at time t and location x), i.e.

$$\lambda_i(t,x) = \frac{\partial \Psi}{\partial y(t,x)} \tag{11}$$

are the solutions of the following continuous adjoint PDE:

$$
\begin{aligned}
&\frac{\partial \lambda_i}{\partial t} = -\nabla \cdot (\vec{u}\lambda_i) - \nabla \cdot \left(\rho K \cdot \nabla \frac{\lambda_i}{\rho}\right) - (J^{\mathrm{T}}(\rho y) \cdot \lambda)_i - \phi_i \\
&\lambda_i(t^{\mathrm{F}}, x) = \lambda_i^{\mathrm{F}}(x), \quad t^{\mathrm{F}} \geqslant t \geqslant t^0 \\
&\lambda_i(t,x) = 0 \quad \text{on } \Gamma^{\mathrm{IN}} \\
&u_n \lambda_i + \rho K_{nn} \frac{\partial(\lambda_i/\rho)}{\partial n} = 0 \quad \text{on } \Gamma^{\mathrm{OUT}} \\
&\rho K_{nn} \frac{\partial(\lambda_i/\rho)}{\partial n} = V_i^{\mathrm{DEP}} \lambda_i \quad \text{on } \Gamma^{\mathrm{GROUND}}
\end{aligned}
\tag{12}
$$

The continuous adjoint PDE is solved backward in time from t^{F} down to t^0. Here $J(y) = \partial f(y)/\partial y$ is the Jacobian of the chemical equation rates. The forcing functions ϕ_i depend on the particular form of the cost functional Ψ. Note that the formulation of the continuous adjoint PDE is based on the concentrations, i.e. on the solution of the forward model PDE (1). Therefore the model (1) needs to be solved first, and its solution stored for all concentrations, times, and locations.

4.4. Adjoint sensitivity analysis results

The adjoint variables are also called *influence functions*, and their distributions in the three-dimensional computation domain, which are available at any instant, provide the essential information for the sensitivity analysis [37,24,113].

For instance, isosurfaces of the ith adjoint variable ($\lambda_i(t,x) = $ constant) delineating "instantaneous areas of influence" may be used to identify locations where perturbations in the concentration of the ith chemical species at time t will produce significant changes in the response function, e.g. the observed ozone level at the receptor site and time. Time integrals of the adjoint variables over the time period of interest

$$\sum_{k=0}^{F} \lambda^k \tag{13}$$

define "integrated areas of influence", i.e. regions where the cumulative effect of concentration changes of the ith species over the interval of interest will affect the target most.

This offers a powerful method to characterize source–receptor relationships. These areas of influence cannot be computed based solely on inverting meteorological fields, due to the influence of turbulent diffusion and complicated chemical reactions.

To illustrate how this information can be used adjoint sensitivity analysis results for a cost function that measures ground level ozone concentration in the Dallas-Fort-Worth (DFW) receptor area using the STEM model [22] are presented in Fig. 5. In order to understand the influence of the meteorological conditions on the adjoint, the adjoint sensitivities of a passive tracer (no chemical reaction or removal) are also presented. Simulations are carried out for a 36-h interval starting at 9:00 EDT July 1st 2004. The scaled adjoint sensitivities of DFW ozone with respect to earlier concentrations of O_3, NO_2, and HCHO are presented. Specifically, we present the "integrated areas of influence", i.e. the time integrals of scaled adjoint sensitivities of DFW ozone. For the tracer calculations the integrated areas of influence for the adjoint sensitivity (without scaling) are shown. The results for the tracer show the maximum influence near the receptor, with structure along the back-trajectory, and spread due to atmospheric dispersion processes. The results for the sensitivities with respect to NO_2 and O_3 show the role of atmospheric chemistry. For these simulation conditions the region of maximum influence of ozone on DFW ozone is found over the southeast tip of Texas. As this air mass is transported during the next 36 hours to DFW the ozone levels are dominated by chemical and removal processes. The sensitivities with respect to NO_2 show the role of chemical processes. The photo-dissociation of NO_2 during the day results in ozone formation. NO_2 values near the surface are influenced by direct emissions and by the nighttime reaction of $O_3 + NO \rightarrow NO_2 + O_2$, which increases NO_2. The net effect of these processes is that the influence of NO_2
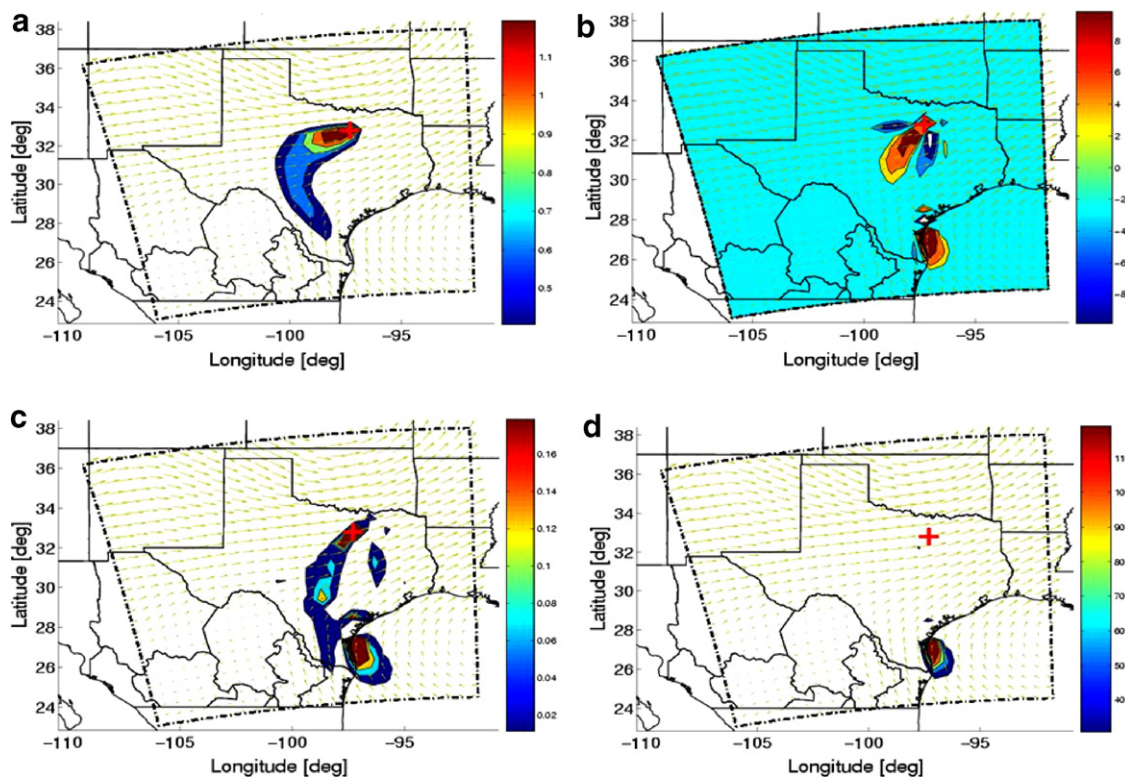

Fig. 5. (a) Tracer; (b) HCHO; (c) NO_2; (d) O_3. Time-integrated areas of influence of various species on the Dallas-Fort-Worth O_3 concentration at 9 pm July 2, 2004.

varies appreciably with distance away from DFW. Formaldehyde shows a different behavior with both positive and negative values, reflecting its nonlinear influence on ambient ozone levels.

4.5. Uncertainty via adjoints

The adjoint sensitivities can also be used to quantify the uncertainty in the response due to uncertainties in the model input [20]. In many practical instances, the true parameter values p^* are not known (e.g. emission rates) and the response calculations $\Psi(p)$ are performed for some nominal parameter values p characterized by uncertainties $\delta p = p - p^*$. The uncertainty in the response functional may be estimated using a truncated Taylor series

$$\delta\Psi = \Psi(p) - \Psi(p^*) \approx \nabla_p \Psi(p) \cdot \delta p - \frac{1}{2}\delta p \cdot \nabla_p^2 \Psi(p) \cdot \delta p \tag{14}$$

First-order derivatives are provided by the adjoint model. The second-order derivative information may be obtained without explicit computation of the Hessian since the Hessian vector products may be evaluated directly using a second-order adjoint model [80].

If the input parameters are viewed as random variables with expected values $\bar{p}, p = \bar{p} + \delta p$, the sensitivities may be used to provide statistical information on the response as a function of input. Using a linear approximation, the mean and the variance of the response are expressed as

$$\overline{\Psi} = \Psi(\bar{p}), \quad \mathrm{Var}(\Psi) = \nabla_p \Psi(\bar{p}) \cdot \Sigma \cdot \nabla_p \Psi(\bar{p}) \tag{15}$$

where $\Sigma = \langle \delta p, \delta p^{\mathrm{T}} \rangle$ is the covariance matrix of the parameters and $\nabla_p \Psi(p)$ is the sensitivity vector evaluated at the nominal parameter values $\bar{p}$.

4.6. Singular vectors and maximal error growth

In order to understand the propagation of errors through the model it is also of interest to quantify the directions (in state space) along which the errors undergo maximal growth when the model evolves from the initial time t^0 to the final time t^F. Assuming that the growth of an initial perturbation δy^0 to the final time follows the tangent linear model, $\delta y^F = M'\delta y^0$, and the perturbation at the initial time is measured using a weight matrix C and at the final time using a weight matrix E, then the directions $s_k(t)$ along which the error growth is maximized are the eigenvectors of the following generalized eigenvalue problem [15]:

$$\sigma^2 = \max_{\delta y^0} \frac{\langle \delta y^F, E\delta y^F \rangle}{\langle \delta y^0, C\delta y^0 \rangle} \iff M'^{\mathrm{T}}EM's_k = \sigma_k^2 C s_k \tag{16}$$
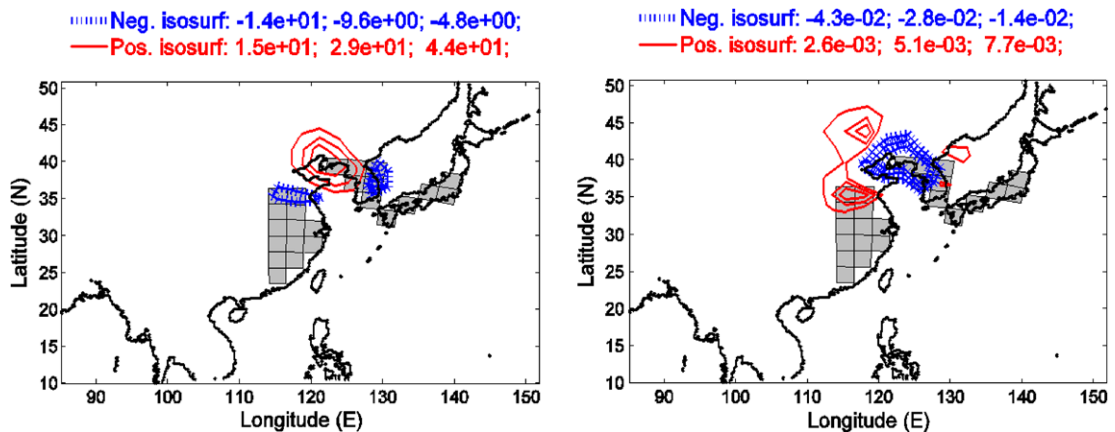

Fig. 6. The O_3 (left) and NO_2 (right) sections of the dominant model singular vectors for a 24 h simulation of chemistry and transport over Asia. The simulated conditions correspond to March 4, 2001. The error norm at the final time is focused on the ground level O_3 and NO_2 over China, Korea, and Japan (grey area).

In [85] the computation of singular vectors for atmospheric chemical transport models was studied. The study found that singular vectors are shaped by both the meteorology and chemistry. An example is given in Fig. 6, where the uncertainty norm at the final time measures the O_3 and NO_2 ground level concentrations over China, Korea, and Japan. The singular values decrease rapidly and a few modes ($\sim$40) are sufficient to capture uncertainty in ground level concentrations over the grey area. The singular vectors depend on the chemical interactions, as illustrated by the different shapes of the O_3 and NO_2 sections.

Singular vectors can be used to help select the ensemble members in an advanced data assimilation methods, and in the design of observing networks (as discussed in Sections 5.3 and 6.2.2).

5. Directions for better air quality forecasts

5.1. Ensemble forecasts

An important technique to deal with the underlying uncertainty in air quality modeling is to make forecasts using ensembles of predictions. Ensemble techniques are commonly used to improve the forecast ability of weather models [73]. The application of ensemble techniques to air quality forecasts is very recent [43,101,91]. As part of a collective, informal model verification project within the ICARTT/NEAQS-2004 study, forecasts of several key meteorological, radiation, and gas-phase atmospheric constituents were gathered in near real time (typically 4- to 10-h computational delay) from seven CTMs and used to evaluate forecast skill for predicting surface ozone [94]. The major intent of this study was to critically examine the usefulness of the ensemble forecast relative to its individual members, and to provide a reference for future real-time air quality (AQ) ensemble forecasts. Each individual CTM showed better predictive skill than persistence. However, the ensemble predictions based on the mean of the seven models was found to have significantly more temporal correlation to the observed daily maximum 1-hour average and maximum 8-hour average O_3 concentrations than any individual model. Illustrative results are shown in Fig. 7. Ensembles using simple bias correction algorithms were also evaluated and found to improve the forecast skill [94,101,126].

5.2. Chemical data assimilation

For the predictive capabilities of CTMs to improve, they must be better constrained through the use of observational data. The close integration of observational data is recognized as essential in weather/climate analysis, and it is accomplished by a mature experience/infrastructure in data assimilation – the process by which models use measurements to produce an optimal representation of the state of the atmosphere. This is equally desirable in CTMs.
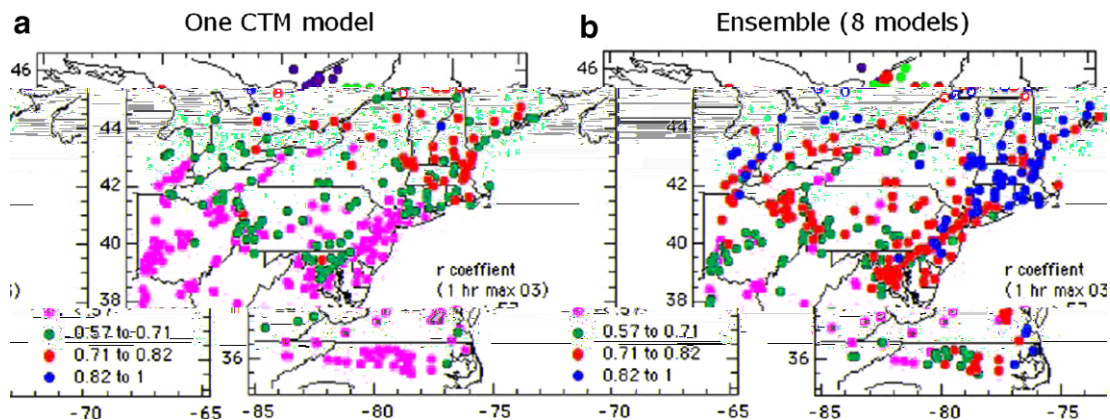

Fig. 7. Comparison of forecast skills for the summer of 2004. Shown are calculated correlation coefficients for predicted and observed surface ozone (hourly) at the Air Now monitoring sites. (a) The forecasts of the STEM model; (b) forecasts skill using an eight member ensemble.

Data assimilation combines information from three different sources: the physical and chemical laws of evolution (encapsulated in the model), the reality (as captured by the observations), and the current best estimate of the distribution of pollutants in the atmosphere (all with associated errors). As more chemical observations in the troposphere are becoming available, chemical data assimilation is expected to play an essential role in air quality forecasting, similar to the role it has in numerical weather prediction.

Advanced assimilation techniques fall within the general categories of variational (3D-Var, 4D-Var) and Kalman filter-based methods, which have been developed in the framework of optimal estimation theory. The variational data assimilation approach seeks to minimize a cost functional that measures the distance from measurements and the ''background'' estimate of the true state. In the 3D-VAR method [87,81,120] the observations are processed sequentially in time. The 4D-Var [35,46,48,49,56,106] generalizes this method by considering observations that are distributed in time. These methods have been successfully applied in meteorology and oceanography [99], but they are just beginning to be used in nonlinear atmospheric chemical models [96,47,114,26]. Recently the principle of maximum entropy was employed in data assimilation using an atmospheric tracer [12,13]. The method is equivalent to 4D-Var when the error distributions of both the source prior estimates and observations are Gaussian. When chemical transformations and interactions are considered, the complexity of the implementation and the computational cost of the data assimilation are highly increased. Some of the important challenges in chemical data assimilation include:

(1) memory shortage ($\sim$100 concentrations of various species at each grid points, check-pointing required);
(2) stiff differential equations ($>$200 various chemical reactions coupled together, lifetimes of different species vary from seconds to months);
(3) chemical observations are limited, compared to meteorological data;
(4) emission inventories are often out-dated, and uncertainties are not well-quantified.

A discussion of current approaches follows.

5.2.1. Problem formulation

Consider the chemical transport model (1) discretized in time and space (2). Observations of quantities that depend on system state are available at discrete times t^k

$$y_{\text{obs}}^k = h(y^k) + \varepsilon_{\text{obs}}^k \approx H_k y^k + \varepsilon_{\text{obs}}^k, \quad \langle \varepsilon_{\text{obs}}^k \rangle = 0, \quad \left\langle (\varepsilon_{\text{obs}}^k)(\varepsilon_{\text{obs}}^k)^{\text{T}} \right\rangle = O_k \tag{17}$$

where $y_{\text{obs}}^k \in \Re^m$ is the observation vector at t^k, h is the (model equivalent) observation operator and H_k is the linearization of h about the solution y^k. Each observation is corrupted by observational (measurement and representativeness) errors $\varepsilon_{\text{obs}}^k \in \Re^m$ [28]. We denote by $\langle \cdot \rangle$ the ensemble average over the uncertainty space. The observational error is usually considered to have a Gaussian distribution with zero mean and a known covariance matrix O_k.

The aim of data assimilation is to find $P[y(t^k)|y_{\text{obs}}^k \cdots y_{\text{obs}}^0]$, the PDF of the true state at time t^k conditioned by all previous observations (including the most recent one). From Bayes' rule

$$P[y(t^k)|y_{\text{obs}}^k \cdots y_{\text{obs}}^0] = \frac{P[y_{\text{obs}}^k|y(t^k)] \cdot P[y(t^k)|y_{\text{obs}}^{k-1} \cdots y_{\text{obs}}^0]}{\int P[y_{\text{obs}}^k|y] \cdot P[y|y_{\text{obs}}^{k-1} \cdots y_{\text{obs}}^0] \, \mathrm{d}y}, \tag{18}$$

where $P[y_{\text{obs}}^k|y(t^k)] = P(\varepsilon_{\text{obs}}^k)$ is the PDF of the latest observational error. $P[y(t^k)|y_{\text{obs}}^{k-1} \cdots y_{\text{obs}}^0]$ is the ''model forecast PDF'' (conditioned by all previous observations minus the most recent one) and $P[y(t^k)|y_{\text{obs}}^k \cdots y_{\text{obs}}^0]$ is the ''assimilated PDF''.

5.2.2. Chemical data assimilation using 4D-Var

In the 4D-Var approach an optimal solution is sought by adjusting chosen parameters according to available measurements in the analysis time interval. Such parameters are often called control variables and they may include initial concentrations, emission rates, concentrations and fluxes at domain boundaries, and other physical or chemical parameters. The optimal solution of the control variables minimizes a cost functional that is generally defined as

$$\Psi = \frac{1}{2}[y^0 - y_b^0]^{\mathrm{T}} B^{-1} [y^0 - y_b^0] + \frac{1}{2}[p - p_b]^{\mathrm{T}} P^{-1}[p - p_b] + \frac{1}{2}[h(y) - y_{\mathrm{obs}}]^{\mathrm{T}} O^{-1}[h(y) - y_{\mathrm{obs}}] \tag{19}$$

where B, P, and O are error covariance matrices in discrete spaces for background initial values y_b^0, parameters p_b, and observations y_{obs}, respectively. h is a projection operator, used to calculate the observation vector $y^{\mathrm{obs}}(t)$ from the model state variables.

The optimal solution depends on the uncertainty of both observations and control variables, which are represented by the error covariance matrices, B, P, and O. As observational errors are often uncorrelated with each other, O is typically assumed as a diagonal matrix. The complexity of P depends on the choices of control parameters. The background error covariance matrix B is often correlated in space and between different species. An accurate estimation of the background error covariance matrix is difficult to provide and, given its huge dimensionality, simplifying approximations are required for the practical implementation. Information on the error statistics may be obtained using differences between forecasts with different initialization time (NMC method [104]) or ensemble methods based on a perturbed forecast-analysis system [55]. Recent advances in modeling flow-dependent background error variances are discussed in [76]. An autoregressive model was recently introduced to estimate flow-dependent background error covariance for chemical data assimilation [31]. In applications, B is typically expressed as a product of sparse (or rectangular) matrices $B = LL^{\mathrm{T}}$ to reduce the computational burden [56,44,124]. The matrix L can be used as a preconditioner by introducing a new control variable $\hat{c}_0$ defined by $L\hat{c}_0 = (c_0 - c_b)$. Recently, [25] applied Truncated Singular Value Decomposition regularization (TSVD) to implement background error covariance matrix obtained using NMC method.

As described earlier, gradients of the cost functional with respect to all control parameters are calculated simultaneously through the adjoint model. With the gradients, the optimal solution can be found efficiently by applying various minimization routines. Quasi-Newton limited memory L-BFGS [17] is used by most 4D-Var applications. Chai et al. [26] found that adding constraints to the admissible solution space through L-BFGS-B [127] improved the optimization efficiency.

The data assimilation problem is then formulated as an optimization problem

$$\min \Psi(p, y^0) \quad \text{for } p \in P_{\mathrm{ADMISSIBLE}}, \quad y^0 \in Y_{\mathrm{ADMISSIBLE}} \tag{20}$$

The minimization process is computationally demanding, but can be efficiently implemented using adjoint modeling to compute the gradients $\nabla_{y^0}\Psi \in \mathfrak{R}^n$ and $\nabla_p \Psi \in \mathfrak{R}^m$ of the cost functional. To further improve the optimization efficiency, it is possible to perform the minimization in a low-order control space and such strategies were recently investigated in [39,38].

5.2.3. Results with 4D-Var chemical data assimilation

The effect of data assimilation on predicted surface ozone for Texas in July 2004 is shown in Figs. 8–11. In this application surface ozone data (hourly values from 114 stations) from the AirNow network was used, and the control variables were the initial concentrations of all chemical species. The simulation results for July 16, 2004 are compared against the measurements at selected stations in the Dallas Fort Worth area (S1, S2), Houston area (S4, S5), and Austin area (S6, S7). The forward model predictions (without assimilation) capture the main observed features (e.g. high ozone levels around the major metropolitan regions of Texas) as shown in Fig. 9. However as shown in Fig. 10 the forward model has a significant positive bias at low ozone levels and a negative bias at high values. After assimilation, the ozone prediction skill increases significantly and the biases are dramatically reduced. These results demonstrate the effectiveness of 4D-Var in better determining the analysis state. The effect on forecast skill is discussed later.

5.3. Chemical data assimilation using ensemble Kalman filters

5.3.1. Ensemble Kalman filters

The ensemble Kalman filter (EnKF) approach to data assimilation has recently received considerable attention in meteorology. The Kalman filter [72,50,51] solves (18) under the assumptions that the model is linear, and the model analysis state at previous time t^{k-1} is normally distributed with mean y_a^{k-1} and covariance
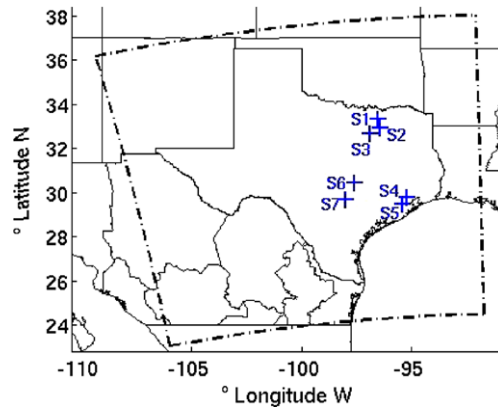
Fig. 8. The selected set of AirNow stations where results are presented.
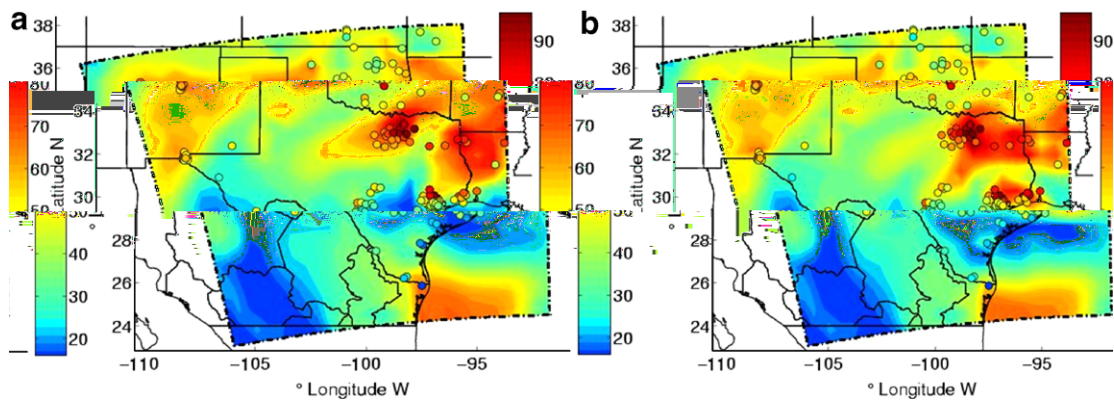

Fig. 9. (a) Original model prediction; (b) model prediction after assimilation. Ground level ozone distribution in East Texas at 6 pm CST July 16, 2004 (a) before data assimilation, and (b) after data assimilation. The colored circles represent the AirNow stations and their measured values. Data assimilation uses only AirNow ozone data and adjusts for the initial concentrations of all chemical species.
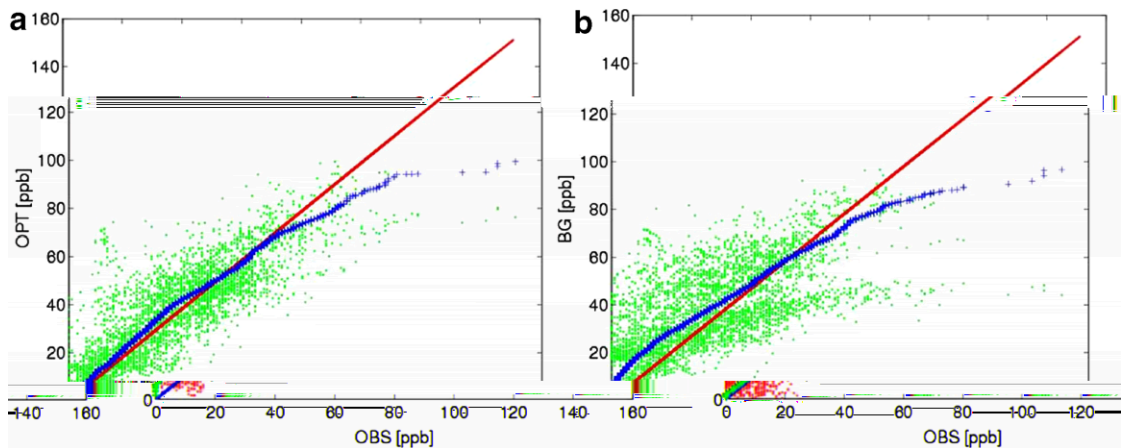

Fig. 10. Scatter– and quantile–quantile plots of model predictions vs. observations (a) for the original model predictions before data assimilation, and (b) after data assimilation. The R^2 measure of model-observations agreement improves considerably.
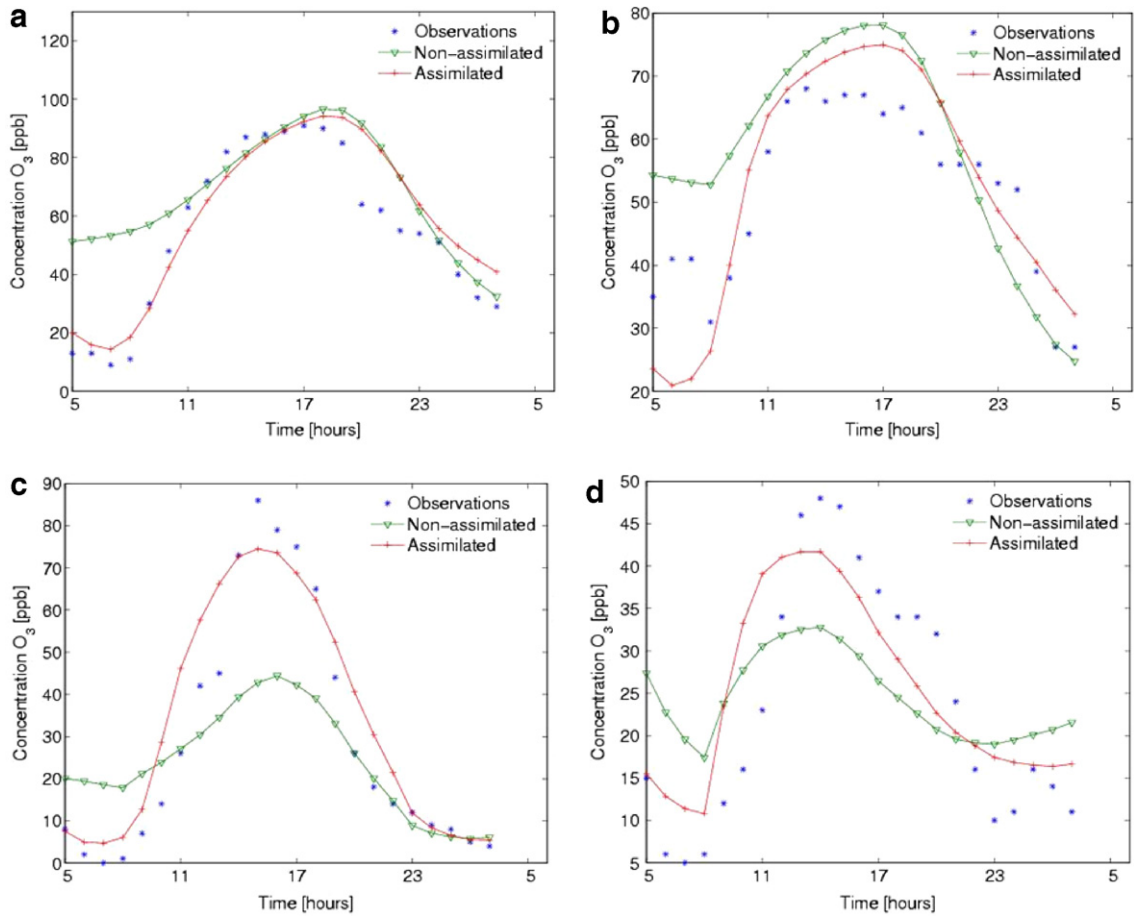
Fig. 11. (a) O_3 at station S1 (DFW area); (b) O_3 at station S3 (DFW area); (c) O_3 at station S4 (Houston area); (d) O_3 at station S7 (Austin area). Time series of ozone concentrations on July 16, 2004. The concentrations are plotted against EDT time. Shown are the measured concentrations, and model predictions before and after data assimilation.

matrix P_a^{k-1}. The Extended Kalman Filter (EKF) allows for nonlinear models and observations by assuming the error propagation is linear (through the tangent linear model) and by linearizing the observation operators, $y_{obs}^k = H_k y^k + \varepsilon_{obs}^k$. However, the (extended) Kalman Filter is impractical for large systems due to the high cost of propagating covariance matrices. A practical approach is provided by the ensemble Kalman Filter (EnKF) [52,16] which estimates covariances through sampling the state space. Consider an ensemble of N states $\{y_a^{k-1}[i]\}_{1 \leqslant i \leqslant N}$ at t^{k-1}. Each of the ensemble states is evolved in time using the model equation to obtain a forecast ensemble at t^k,

$$y_f^k[i] = M(p, y_a^{k-1}[i]), \quad 1 \leqslant i \leqslant N \tag{21}$$

The mean and the covariance of the forecast PDF are approximated by the ensemble statistics

$$\langle y_f^k \rangle = \frac{1}{N} \sum_{i=1}^N y_f^k[i], \quad (P_f^k)_{i,j} = \frac{1}{N-1} \sum_{i=1}^N (y_f^k[i] - \langle y_f^k \rangle)(y_f^k[i] - \langle y_f^k \rangle)^{\mathrm{T}} \tag{22}$$

An ensemble of observation vectors $\{y_{obs}^k[i]\}_{1 \leqslant i \leqslant N}$ is constructed by adding to the most recent observation vector y_{obs}^k perturbations drawn from a normal distribution with zero mean and covariance O_k. Each member of the ensemble is assimilated using the EKF to obtain the ensemble of analyzed states $\{y_a^k[i]\}_{1 \leqslant i \leqslant N}$

$$y_a^k[i] = y_f^k[i] + P_f^k H_k^{\mathrm{T}}(O_k + H_k P_f^k H_k^{\mathrm{T}})^{-1}(y_{obs}^k[i] - H_k y_f^k[i]) \tag{23}$$

The ensemble mean and covariance describe the PDF of the assimilated field. The cost of updating the covariance matrix is that of N model evaluations. The ensemble implicitly describes a density function that can be non-Gaussian. Experience gained in numerical weather prediction indicates that relatively small ensembles (50–100 members) are sufficient to accurately capture this density function [67]. Extensions of this approach proposed in the literature include the Ensemble Kalman Smoother [54], the 4D-EnKF method [69], the Ensemble Transform Kalman Filter [11], the hybrid approach [62] and ensemble nonlinear filters [5,4,105].

The application of EnKF presents several challenges: (1) the rank of estimated covariance matrix is (much) smaller than its dimension [68]; (2) the random errors in the statistically estimated covariance decrease only by the square-root of the ensemble size; (3) the subspace spanned by random vectors for explaining forecast error is not optimal [65]; and (4) the estimation and correct treatment of model errors is possible but difficult [41,117,66,62,7]. In addition, a careful implementation is required for efficiency [68].

In spite of these challenges, EnKF has many attractive features including: (1) it is able to propagate the PDFs through highly nonlinear systems; (2) it does not require additional modeling efforts such as the construction of tangent linear model and its adjoint; and (3) the method is highly parallelizable.

5.3.2. Results with ensemble-based chemical data assimilation

The performance of EnKF applied to chemical data assimilation has recently been reported [112,32,33]. To illustrate we show results for a simulation of air pollution in North-Eastern United States in July 2004 as shown in Fig. 12 (the dash-dotted line delimits the computational domain). The initial concentrations, meteorological fields, boundary values, and emission rates are all prescribed (after being computed off-line) and correspond to the ICARTT (International Consortium for Atmospheric Research on transport and Transformation) [118]
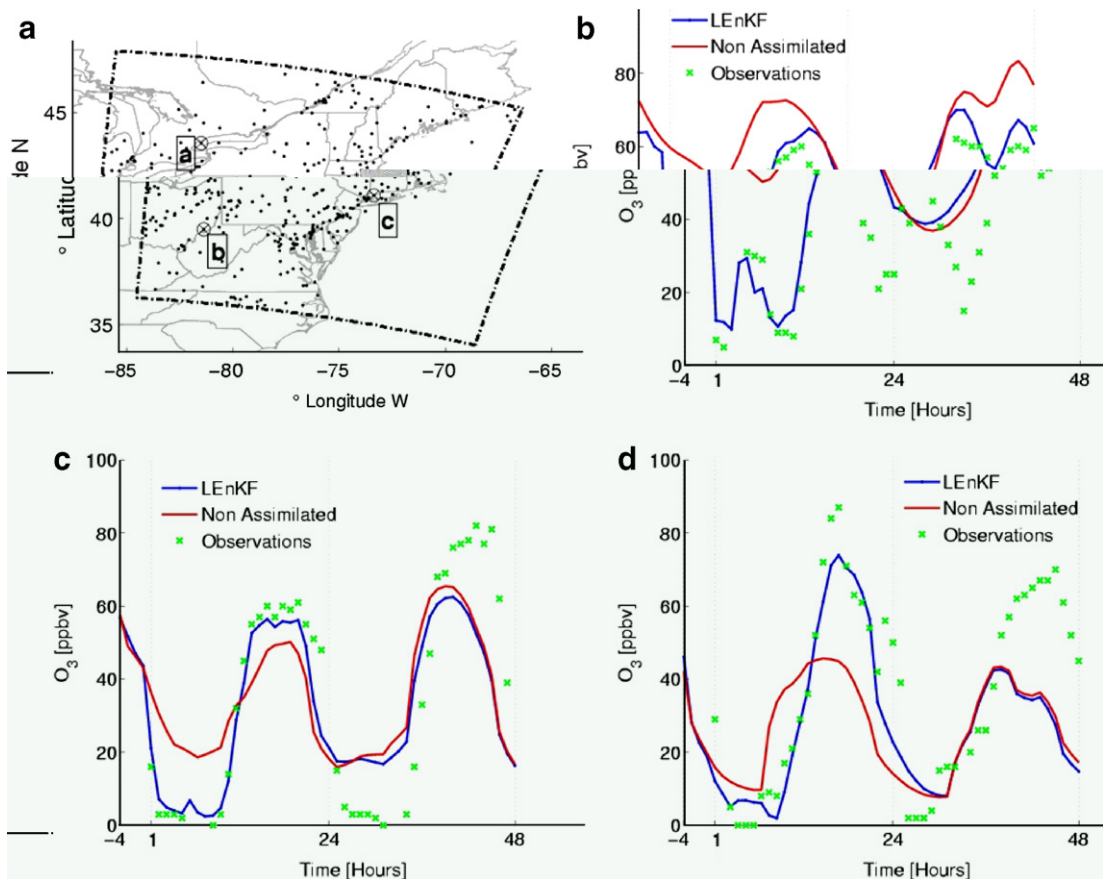

Fig. 12. The location of AirNow stations and the time evolution of ozone at three selected stations.

campaign in summer 2004. The observations used for data assimilation are ground-level ozone (O_3) measurements taken by the 340 EPA AirNow stations shown in Fig. 12. These observations are available hourly in the assimilation window (0–23 EDT, July 20 2004). After assimilation the model is allowed to evolve in forecast mode for another 24 h. Results for the EnKF as well as for 4D-Var were obtained and compared. Details of the calculations are presented below.

Analysis setting: The "perturbed observations" implementation [53] of the filter is employed. EnKF adjusts the concentration fields of 66 "control" chemical species in each grid point of the domain every hour in the assimilation window. The ensemble size was chosen to be 50 members to provide a good balance between accuracy and computational efficiency. For the 4D-Var application the concentrations of the 66 control chemical species at the beginning of the assimilation window were adjusted.

The initial ensemble: The initial ensemble was sampled following the methods of [60,61]. An autoregressive model of background errors [85,31] was used, which accounted for spatial correlations, distance decay, and chemical lifetime.

Covariance inflation: The "textbook application" of EnKF [53] to this particular scenario lead to filter divergence and a decreasing ability toward the end of the assimilation window. In [32,33] several ways to "inflate" the ensemble covariance in order to prevent filter divergence were investigated. These included: additive inflation [34] (addition of uncorrelated noise to model results), multiplicative inflation [4] (each member's deviation from the ensemble mean is multiplied by a constant), and model-specific inflation (obtained through perturbing key model parameters like the wind field velocities, boundary conditions, and emissions). The results [32,33] found that model-specific inflation best preserves the correlations between various chemical species.

Covariance localization: To alleviate the spurious long-distance correlations (inherent with small size ensembles) each entry in the covariance matrix was multiplied by a Gaussian function with a horizontal de-correlation distance of 270 km and a variable vertical de-correlation distance. The de-correlation distances were obtained experimentally by the NMC method [25].

Illustrative results are presented in Fig. 12. The performance of each data assimilation experiment is measured by the R^2 correlation factor. The correlation between the observations and the model solution in the assimilation window is $R^2 = 0.24$ for the non-assimilated solution, $R^2 = 0.52$ for 4D-Var (results not shown), and $R^2 \approx 0.8$–0.9 for EnKF (with various forms of covariance inflation and localization). The overall behavior of the filter is also shown in Fig. 13, where the distribution of ground level ozone during the afternoon peak as predicted by the model before (Fig. 13(a)) and after assimilation (Fig. 13(b)) are plotted. The assimilated field more closely matches the observations (especially near the west inflow boundary) and displays finer scale structures. The time evolution of ozone concentrations at selected ground stations (Fig. 12) shows how the
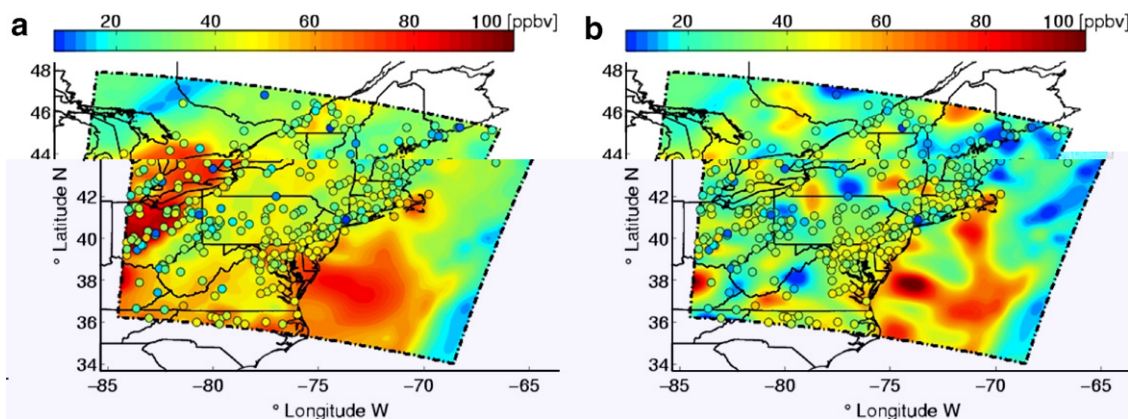

Fig. 13. Ground-level ozone at 14:00 EDT on July 20, 2004 as predicted by the model (a) without data assimilation, and (b) with data assimilation. The data is provided by the AirNow network (shown as circles colored by the measured ozone level).

assimilated ozone series follow the observations much closer than the non-assimilated ones in the analysis window.

The impact of data assimilation on the forecast skill is also shown. The period from 24 to 48 h represents the forecast. As shown the effect of assimilation of surface ozone on forecast improvements is mixed. At station A the effects are significant, while at the other sites the effects are slight. This is due in part to the fact that only ground level observations are assimilated and the vertical profiles are not constrained at all. This is also due to the fact that near surface ozone levels are strongly dependent on chemical production/destruction processes involving a variety of precursor species, as shown in Fig. 2 and by the sensitivity results in Fig. 17. It should be noted that the current data assimilation only adjusts the concentration fields. If the emission inventories of ozone precursors are adjusted as well, a larger impact of data assimilation on the forecast skill is expected.

6. Further improvements in forecasting

6.1. Incorporating emissions into the analysis

One of the main differences between weather and chemical-weather forecasting is the strong local forcing due to emissions, typically the largest source of uncertainty in the predictions. Thus an increase in air quality prediction skill requires better estimates of emissions. This is challenging due to the complexity and uncertainties associated with the bottom-up emission estimates (i.e. inventories built on activity information, e.g. emission factors, fuel use and type, control technologies, and their regional variation), the transient nature of some emissions (fires and dust storms), and their ever changing nature (e.g. trends due to policy and/or technology changes) [119]. Improvements in emissions will also come from the closer integration of observations and models.

Observations can provide a top-down constraint on emissions as illustrated in Fig. 14. In this approach (also referred to as inverse modeling of emissions) [102,6,100,59], the emissions are adjusted to best match the model predictions with the observations, within error estimates. The same data assimilation techniques discussed above can encompass emission estimates. To illustrate the use of 4D-Var to invert for emissions, scaling factors applied to the background (a priori values) of ground level emissions can be introduced

$$E_s(x_i, y_j, t) = \alpha_{i,j,s} E_s^B(x_i, y_j, t) \tag{24}$$

In the simplest case the scaling factors can be held constant throughout the entire simulation interval; i.e. the time-dependent emission profile of species s at location (x_i, y_j) is scaled by the constant factor $\alpha_{i,j,s}$; the scaled emissions have the same temporal evolution profile, but have a different magnitude than the original emission profile. The base case is characterized by constant scaling factors $\alpha_{i,j,s} = 1$. The data assimilation process will update the scaling factors in order to minimize the model-observations mismatch. The minimization problem to be solved is

$$\min \quad \Psi(\alpha) = \frac{1}{2}(\alpha - 1)^{\mathrm{T}} P^{-1}(\alpha - 1) + \frac{\gamma}{2}\|\Delta(\alpha - 1)\|^2 + \frac{1}{2}\sum_{k=0}^{N}(H_k y^k - y_{\mathrm{obs}}^k)^{\mathrm{T}} O^{-1}(H_k y^k - y_{\mathrm{obs}}^k) \tag{25}$$

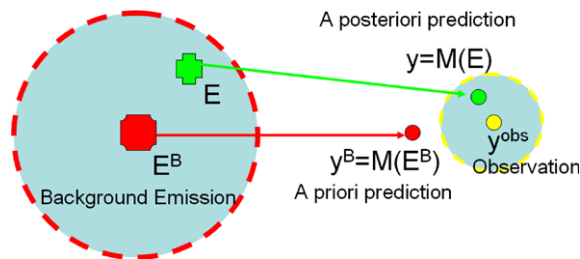subject to $\alpha_{\min} \leqslant \alpha \leqslant \alpha_{\max}$

Fig. 14. A-basic methodology of top-down estimates of emissions.

The first term is the ''background term'' in 4D-Var and penalizes the departure of the scaling factors from the ''best guess'' value of 1. The second term is a regularization term. The Laplacian of the scaling factor ($\Delta = \partial^2/\partial x^2 + \partial^2/\partial y^2$) is large if the scaling factor changes appreciably from one location to another. The introduction of the regularization term in the cost functional favors a smooth spatial profile of the correction factors, by penalizing jumps in the profile value. The strength of the penalty is given by the (adjustable) constant γ. The last term in the cost function measures the mismatch between model predictions and observations. The correction factors are restricted to an interval $[\alpha_{min}, \alpha_{max}]$ which is predetermined to contain ''reasonable'' correction values. Examples of 4D-Var applied to the inverse modeling of mercury emissions are shown in Fig. 15, where Hg measurements on-board the C-130 aircraft during the ACE-Asia (April 2001) experiment were used to find the optimal emission scaling factors [103].

Another direction that is promising is to incorporate emissions as control variables, along with initial conditions and with boundary conditions, in the assimilation cycle. Unlike the traditional inverse modeling approach where the emissions are adjusted and then used in subsequent model runs, in this manner the emissions are adjusted each assimilation cycle. The importance of including the emission estimates as a control variable in order to improve prediction skill in air quality has been reported by Elbern et al. [49], where they show a marked improvement in air quality forecast skill when emissions and initial conditions are simultaneously treated as controls.

6.2. The role of chemical observations

As discussed throughout this paper, improved predictions require a closer integration of measurements with models. The weather forecast system is supported by a comprehensive observing system designed to improve forecasting skill. No such system exists to support air quality forecasts. The chemical observations presently available were designed largely to monitor environmental compliance and not to enhance predictive skill. However that opens the question as to what chemical data is needed to improve the predictions? The chemical data assimilation techniques can be used to help address this issue.

6.2.1. What observations are needed?

Due to the tight coupling in the chemical processes in the environment, information on multiple species is required to constrain the system. This can be illustrated using adjoint sensitivity results previously discussed in Section 4 [26]. Fig. 16 shows the impacts on the prediction of ozone and PAN (peroxyacetlynitrate formed by the reaction of NO_2 with RO_2 radicals arising from hydrocarbon oxidation) of assimilating various combinations of species (including ozone, PAN, and various nitrogen species involved in the photochemical oxidant cycle, see Fig. 2). The results clearly depend on what observations are assimilated (and which control variables are used). Guidance into what observed quantities and which controls to use can be provided through the
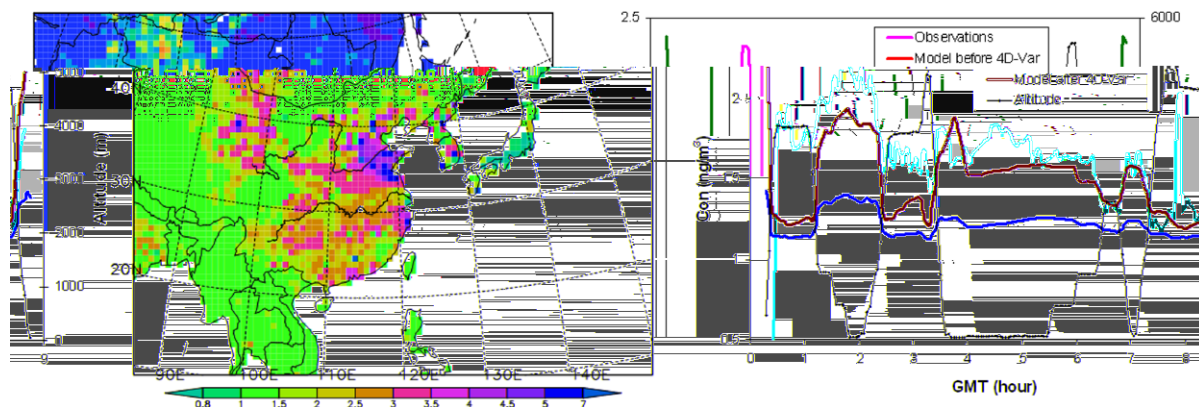

Fig. 15. Optimal mercury emission scaling factors obtained using the 4D-Var approach and the mercury measurements on board the C-130 during the Ace-Asia experiment. Results are for a month-long assimilation window (April 2001).
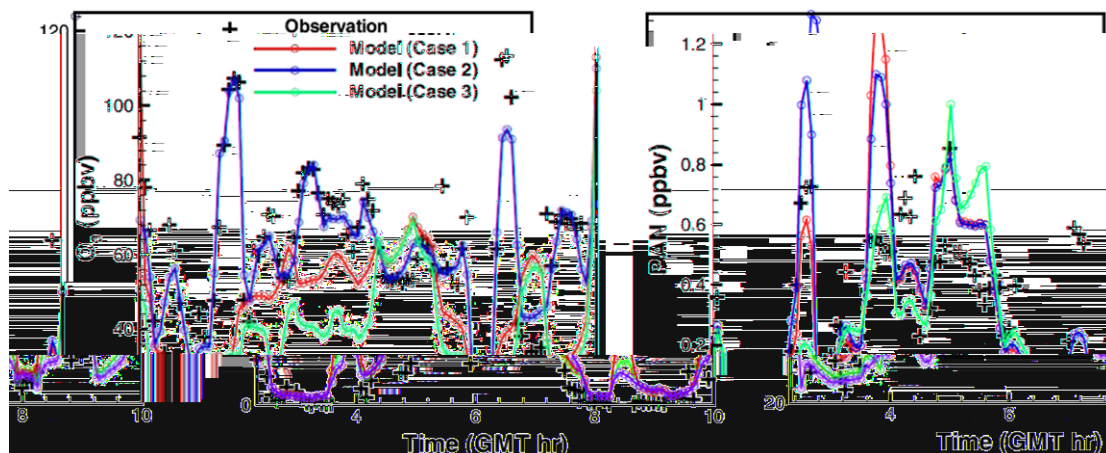
Fig. 16. Comparison of model predictions between three assimilation tests. The measurements that were assimilated: case 1, NOy; case 2, O$_3$, NO, NO$_2$, HNO$_3$, PAN, and RNO$_3$; case 3, NOy, NO, NO$_2$, HNO$_3$, PAN, and RNO$_3$. All measurements are from the P3-B. Observation uncertainties assigned for O$_3$, NO, NO$_2$, NOy, HNO$_3$, PAN, and RNO$_3$ are 8%, 20%, 20%, 18%, 100%, 100%, and 100%, respectively.

adjoint sensitivity analysis. The sensitivity of ozone to initial conditions in this region as a function of height is shown in Fig. 17. Ozone is shown to be dependent not only on its own initial condition, but also on those precursor species for which the photochemical oxidant cycle leads to ozone production/destruction (for which there are many). The sensitivities also are shown to vary significantly with height. These results illustrate the challenge in designing observing systems to aid for air quality prediction, but clearly indicate the need to include observations of multiple species and information at and above the surface. Most recently Chai et al. [25] have demonstrated this fact by systematically assimilating a variety of ozone measurements during
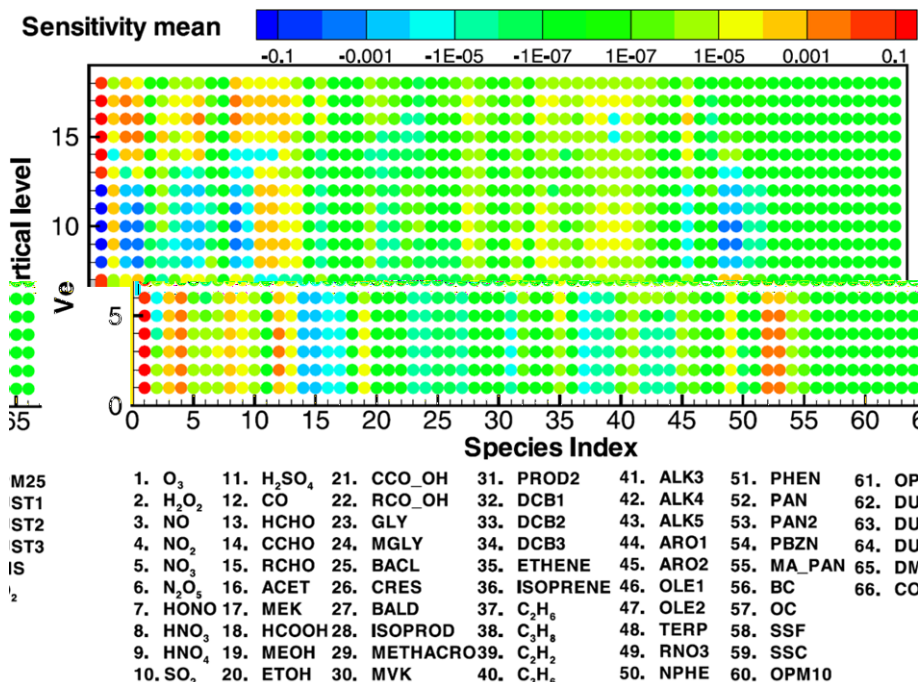

Fig. 17. Sensitivity of ozone predictions to initial conditions.

the recent ICARTT experiment. They evaluate ozone measurements including surface observations, in situ on-board aircraft, airborne ozone lidars, and ozonesondes. Illustrative results are shown in Fig. 18, where the combined effect of surface and upper air data are able to provide a much better representation of the ozone distributions. More formal techniques to design observing systems are needed and are being developed. Examples are discussed below.

6.2.2. Optimal placement of observations

The discussion to this point has looked at how CTMs can use observations to improve predictions. But another important informational loop (see Fig. 1) is the one from the model to the observations: i.e. the model can be used to configure the observational network such that, after a data assimilation cycle, the new observations lead to a significant reduction in the forecast uncertainty (or the uncertainty of specific aspects of the forecast). This is called the *targeted observations* technique. Different techniques for the placement of observations in the context of numerical weather prediction models are discussed in [14,90,77,57,88,83,10]. Studies performed during field experiments revealed the potential benefits that may be achieved using adaptive observations as well as various practical issues and shortcomings of the current targeting methodologies. The design of adaptive strategies must account for various factors such as: the forecast model details, the magnitude of the uncertainty in the initial conditions [88], the uncertainty growth [107], the data assimilation scheme used to provide the initial conditions [9], the configuration of the existing observational network [98], the number of additional observational resources to be allocated.

The adjoint sensitivities discussed earlier can be used to help target observations. In the adjoint sensitivity approach targeted observations are identified using the gradient of a verification functional $J_v(y)$ defined in terms of the forecast at a future verification time t^v over a spatial domain of interest D_v [78]. The forecast $J_v(y)$ at t^v is viewed as a function of the model state at the targeting instant $t^i < t^v$ and the gradient fields $\nabla_{y^i} J_v$ are used to identify areas where errors in the model state at t^i have the most significant impact on the forecast at t^v. Targeted observations at t^i are placed at spatial locations where an appropriate gradient norm $\|\nabla_{y^i} J_v\|$ takes maximal values. Ideally, one would like to evaluate the sensitivity of the *forecast error*
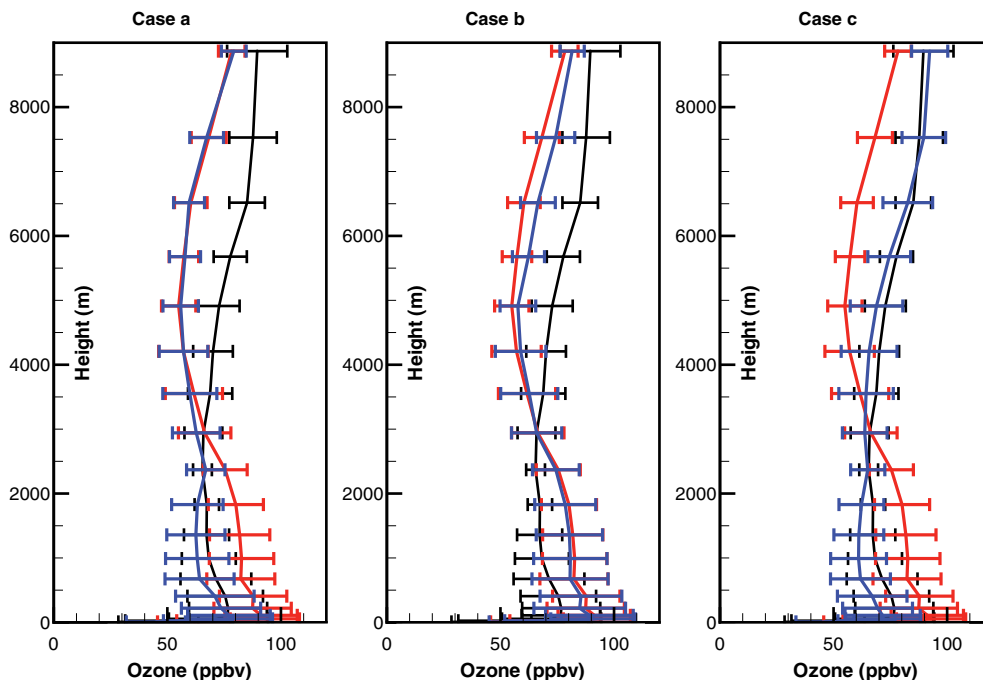

Fig. 18. Domain-averaged vertical profiles (with standard deviation) of the ozone observations (black) and the corresponding predictions before (red) and after assimilation (blue). Case a: AirNow surface measurements; Case b: DC-8 aircraft measurement; Case c: all available measurements. (For interpretation of the references in colour in this figure legend, the reader is referred to the web version of this article.)

with respect to the model state at the targeting time. This may be achieved in a posteriori analysis and data assimilation experiments that are used to provide valuable insight on the benefits and shortcomings of various targeted observations strategies. Langland and Baker use forecasts of different lengths that verify at the same time to define J_v and to assess the observation impact on the forecast error [77].

For a priori *experimental planning* the forecast error at t^v is not known when selecting targets (planning stage), nor are the values of future observational data to be assimilated. Only the location of the future observations provided by the routine observational network (e.g. satellite data) can be specified. In this case the functional J_v must be based on the forecast alone $J_v = J_v(y^v)$.

The design of adaptive observations methodology within the 4D-Var chemical data assimilation framework was discussed in [37,40]. In their work influence functions were used to identify the domain of influence associated with observations distributed in time and space and to account for data interactions within the targeted observations procedure. Data void sensitive regions at targeting instant t^i are identified using a periodic update of the adjoint sensitivity field $\|\nabla_{y^i} J_v\|$ that takes into consideration all observations already located. In this way additional observational resources are deployed at locations where the sensitivity $\|\nabla_{y^i} J_v\|$ is large and little additional information may be obtained from previously located observations. Using this procedure the redundancy between time distributed targeted and conventional observations is minimized.

In [84] an approach based on singular vectors to identify the most sensitive regions and to optimally configure the chemical observational network was proposed. In this approach a vector is defined whose components measure the perturbation energy impact on the verification area at the verification time

$$T = \sum_{k \geqslant 1} \frac{\sigma_k^2}{\sigma_{\max}^2} s_k^2 \qquad (26)$$

This vector is based on the dominant singular vectors s_k and the corresponding singular values σ_k (scaled by the maximum singular value). In practice the summation is only performed for the first few dominant singular vectors. The chemical observations are placed in the locations where the T has maximal values.

An example is given in Fig. 19. The East Asia simulation corresponds to conditions present on March 2–4, 2001. We seek to optimally place observations in order to minimize the uncertainty in the prediction of ground level ozone above Korea (shown in grey) at 0 GMT, March 4, 2001. The optimal location of observations as given by the criterion (26) is different for different chemical species. Also, the optimal locations change with time; Fig. 19 shows the locations for 6–48 h before the verification time.
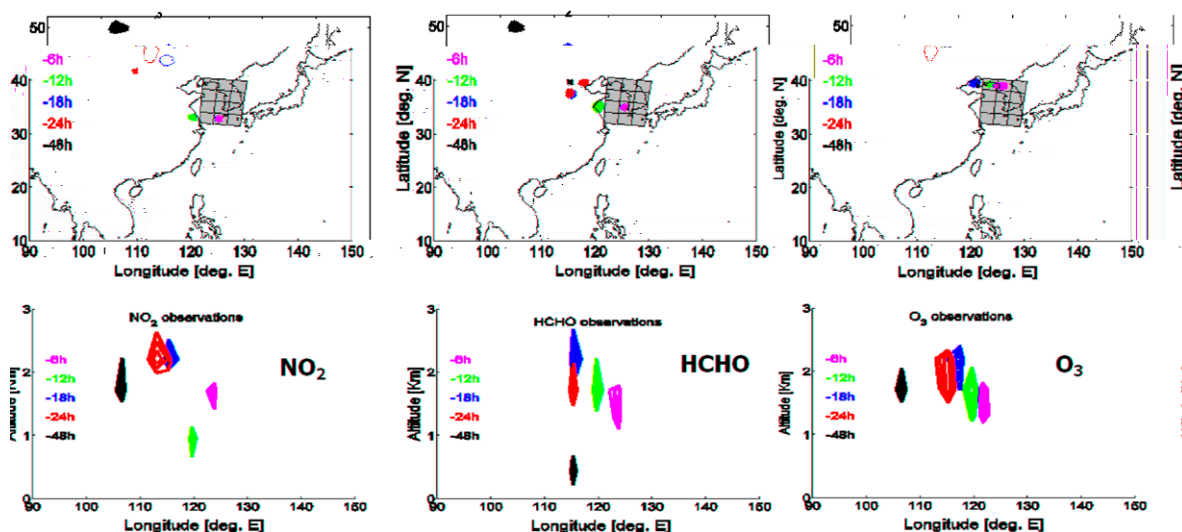

Fig. 19. Optimal location of O_3, NO_2, and HCHO observations to improve predictions of ground level Korean ozone (grey area). Locations of observations are shown at 6, 12, 18, 24, and 48 h before the verification time. Note that different chemical species have to be measured at different locations according to the proposed criterion.

Despite recent advances in the theoretical formulation and implementation of targeting methods, the problem of the optimal adaptive sampling is a young, dynamically evolving discipline, and many open questions remain to be addressed. In particular, the interaction between the sampling strategy and other observing systems in the vicinity, as well as the influence of the background error, have not been properly investigated. These techniques can also be used to help guide the development of future observational strategies including satellite sensor development.

7. Computational aspects

Improvements in air quality prediction have also (and will continue to) come from improved numerical tools. The requirements to use CTMs for urban to global scale applications, to couple chemistry with weather and climate, and to incorporate data assimilation place even more demands for computational efficiency and accuracy. Here we illustrate a few of the computational aspects of air quality prediction. Further details can be found in [27,128], and references therein.

7.1. Stiff chemical equations

The atmospheric chemical processes are tightly coupled and non-linear, and present computational challenges for both forward simulations and for chemical data assimilation. The chemical kinetic processes that take place at each spatial location in the atmosphere are described by a nonlinear system of very stiff ordinary differential equations. To ease model modifications of chemical mechanisms and numerical methods, and to facilitate benchmarking studies, software tools have been developed. One example widely used in air quality modeling is the kinetic preprocessor KPP [42,113,116]. Taking a set of chemical reactions and their rate coefficients as input, KPP automatically generates Fortran90, Fortran77, Matlab, or C code for the temporal integration of the kinetic system. Efficiency is obtained by carefully exploiting the sparsity structures of the Jacobian and of the Hessian. A comprehensive suite of stiff numerical integrators is provided, including methods of Runge Kutta, Rosenbrock, and linear multi-step type. Moreover, KPP can be used to generate the tangent linear model, as well as the continuous and discrete adjoint models of the chemical system.

7.2. Discrete adjoints of numerical advection schemes

As in weather prediction problems, numerical techniques for the convection-diffusion processes play an important role, and the application of inverse techniques places additional demands on the properties of the methods. Studies in [3,122,123] have shown that the construction of discrete adjoints for hyperbolic PDEs (like the advection equation) poses specific challenges. The solution of inverse problems with the convection-diffusion operator was analyzed in detail in [86], where some of the difficulties associated with the behavior of discrete adjoints for numerical advection schemes were discussed. They found that the discrete adjoint of a numerical advection scheme can become pointwise inconsistent with the adjoint advection PDE near the grid points where the forward scheme changes its computational pattern. Such changes in the computational pattern are due to changes in upwind direction, and numerical treatment of boundary conditions (i.e. the change from a high order, large stencil scheme inside the domain to a low order, short stencil scheme near inflow boundaries). This behavior is illustrated in Fig. 20(a), where the discrete adjoint (blue)[1] shows distinct spikes near the boundaries and near the central point where the upwind direction changes. These spikes are not present in the solution of the adjoint PDE (red). Moreover, popular nonlinear advection schemes use flux or slope limiters to prevent spurious wiggles in the forward solution. When these limiters are active a pseudo-source is introduced in the discrete adjoint equation. This is illustrated in Fig. 20(b), where spikes due to pseudo-sources are formed in the discrete adjoint (blue) near the areas where the forward solution (green) has sharp gradients and the limiter is active (black). Again these spikes are not present in the solution of the adjoint advection PDE (red). Future work is needed to analyze the weak convergence of discrete adjoints to the solution of

---

[1] For interpretation of color in Fig. 20, the reader is referred to the web version of this article.
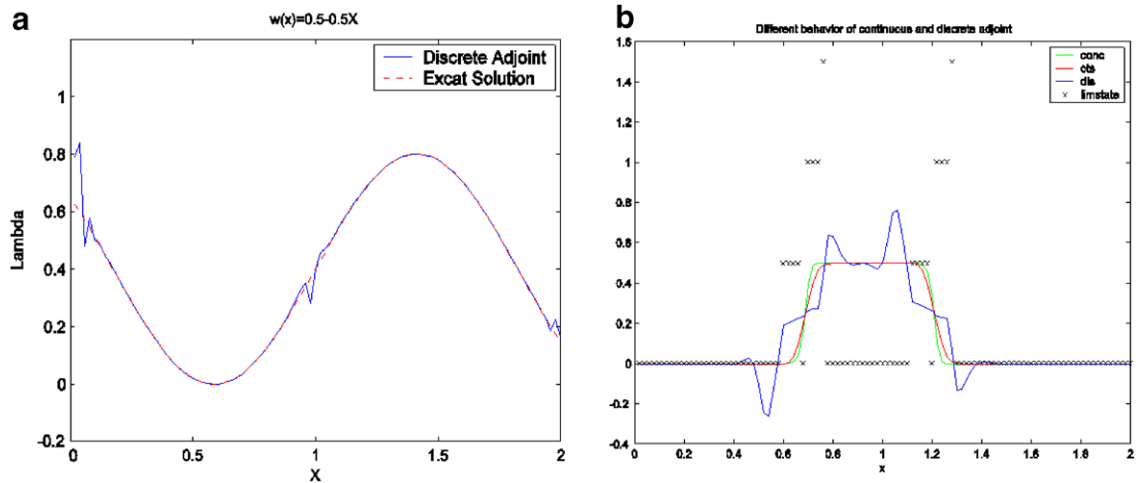
Fig. 20. (a) The discrete adjoint of a third-order, upwind finite difference scheme is point-wise inconsistent with the continuous adjoint PDE near the points where the upwind direction changes (near $x = 1$), and near the inflow boundaries where the numerical scheme is changed. (b) The discrete adjoints of van Leer slope limited scheme are point-wise inconsistent with the continuous adjoint PDE near the points where the limiter is active.

adjoint PDEs in the hyperbolic case, and to fully understand the impact of nonlinearity in advection numerical schemes on the construction of adjoints.

7.3. High performance computing

Since CTMs are very computationally intensive, an essential ingredient in improving air quality predictions is harnessing the power of parallel computers. This is particularly important in the data assimilation context, where 4D-Var applications typically increase the simulation times by factors of 50–80 over that for the forward model. An example of a tool developed to facilitate air quality simulation on parallel computers is the PAQMSG communication library [97]. In [21] a parallel two-level checkpointing scheme for the implementation of the adjoint model which is well suited for clusters was developed using PAQMSG. During the forward run each processor stores the local part of the forward solution vector on the local hard drive (as shown in Fig 21); this part of the solution is read in by the same processor during the backward in time adjoint model run. This localization of data avoids synchronous bursts of network traffic that would appear during checkpoint reading and writing, and would degrade the performance of the adjoint code.

Advances in high speed computing are also allowing the prediction of global weather forecasts at resolutions sufficient to drive directly air quality predictions (tens of meters). These advances are stimulating at the large operational centers the coupling of air quality predictions with the global meteorological forecasts. However the computational resources allocated to the chemical weather component remain restricted, raising many interesting challenges in regards to simplifications and reductions in the CTMs to fit the air quality prediction elements within the available resources.

7.4. Adaptive mesh refinement

Inadequate grid resolution can be an important source of errors in air pollution modeling where large spatial gradients of tracer concentrations result from the complex interactions between emissions, meteorological conditions, and nonlinear atmospheric chemistry. A popular multi-resolution approach in air pollution and meteorological modeling is static nesting of finer grids into coarser grids. This approach requires a priori knowledge of where to place the high resolution grids inside the modeling domain; but it does not adjust to dynamic changes in the solution during simulation. In [30] the dynamic adaptive mesh refinement (AMR) approach for modeling regional air pollution was explored. The grid adapts dynamically during the simulation, with the purpose of controlling the numerical spatial discretization error. Unlike uniform refine-
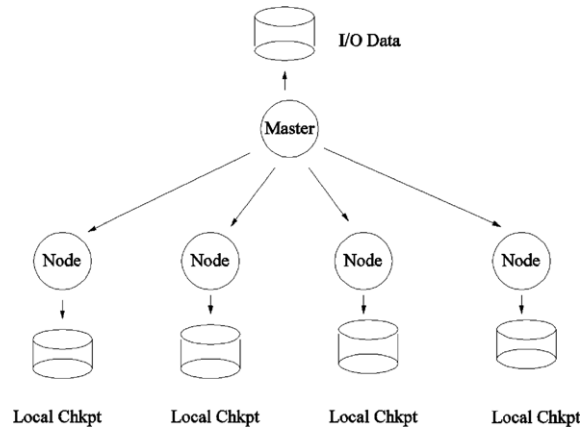
Fig. 21. The distributed checkpointing scheme avoids synchronous bursts of network traffic, and ensures a high parallel efficiency.

ment, adaptive refinement is more economical. Unlike static grid nesting, with AMR it is not necessary to specify in advance which areas need higher resolution; what is required is to define a refinement criterion, which is then used by the code to automatically adjust the grid. An example is shown in Fig. 22. Different error measures to guide the grid refinement have been discussed in [30]. The main conclusion is that an efficient approach to control the numerical errors in ozone predictions is to control the errors in its chemical precursors (NOx, VOCs) and to control the errors upwind of the region of interest. The solution of inverse problems with AMR forward models has not yet been attempted, to our best knowledge.

7.5. Aerosols

While air quality forecasting efforts for ozone have been underway for several years, forecast models for fine particulates (fPM) are more recent and still in an early stage of development. However the need for air quality predictions for particles is high, due to the central role that they play in adverse health, visibility and climate change. The challenges in forecasting particles are similar to those already discussed, but with larger uncertainties in terms of emission estimates, and with additional complexity (e.g. the need to predict both particle composition and size).

To help place the major sources of uncertainty in air quality prediction of aerosols into perspective, a summary of the factor uncertainties of the various processes effecting the prediction of column amounts (a quantity
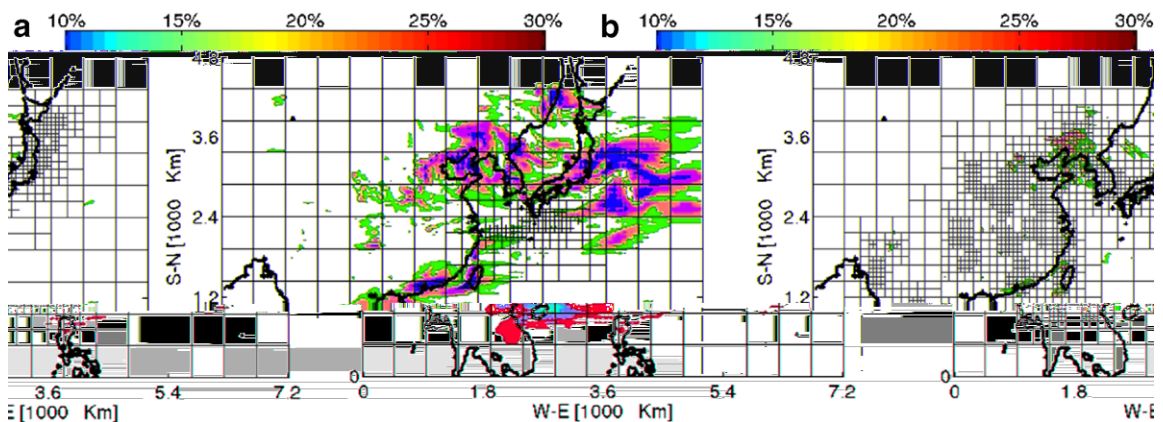

Fig. 22. The grid structure after AMR adaptation for a pollution simulation in east Asia on March 1, 2001. The horizontal grid resolution ranges between 80×80 km and 10×10 km. The grid is automatically refined in areas of higher emissions. (a) The errors in NO_2 for the coarse grid simulation. (b) The NO_2 errors on the adaptive grid.

Table 1
Summary of estimated factor uncertainties in column amounts based on model inter-comparisons, sensitivity studies, and expert opinion

	Emissions	Wet removal	Vertical transport	Chemical formation	Total uncertainty
SO_4*	1.3	1.3	1.5	1.3	1.8
BC	3	2	1.5	–	3.9
OC	3.5	2	1.5	3	6.4
Dust	5	2	1.5	–	6.0
Sea Salt	5	1.3	1.5	–	5.4

SO_4*: non-sea-salt sulfate.

of importance to the prediction of the effect of aerosols on climate) of selected aerosol species are presented in Table 1 (the uncertainties associated with predicting the aerosol composition and size at a specific time and location are higher than those for the column quantities when integrated in time and space) [8]. These estimates are based on model inter-comparisons, sensitivity studies, and expert opinion. These results allow for a qualitative comparison of the sources of uncertainty in the analysis chain. While the relative sources of uncertainty vary from species to species, in general the uncertainties are ranked as follows: emissions > wet removal > chemical formation > vertical transport.

Recently real-time forecasts from four research centers were evaluated over eastern North America during the ICARTT/NEAQS-2004 field experiment [93]. Surprisingly, the 8-h average fPM mass statistics of the predictions were very similar to those for forecasted ozone. However, the models showed little skill in predicting the individual aerosol composition (e.g. sulfate or organics); yet prediction of aerosol composition is important in assessing the impact of aerosol in health and climate. Improved numerical methods and closer integration of models and measurements for aerosol applications are needed and some recent efforts are discussed below.

The populations of particles (aerosols) composed of multiple chemical components are described by the mass density of each component $q_i(m, t)$, $1 \leqslant i \leqslant n$. The total mass of chemical constituent i per unit volume of air, contained in aerosols having particle mass between m and $m + dm$, is $q_i(m, t)dm$ ($\mu g/cm^3$). The mass density of each constituent is changing in time due to coagulation, growth, emission, deposition, convection, diffusion, and chemical and thermodynamic transformations. At each given spatial location the aerosol evolution of particle densities is governed by the following integral partial differential equation called the general dynamic equation (27) [95]

$$\frac{\partial q_i}{\partial t} = \int_0^m \beta(m', m - m') q_i(m', t) \frac{q(m - m', t)}{m - m'} \, dm' - q_i \int_0^\infty \beta(m, m') \frac{q(m', t)}{m'} \, dm'$$

$$+ H_i q - \frac{\partial}{\partial m} (m H q_i) + m_i S - L q_i \tag{27}$$

$$q_i(m, t = t^0) = q_i^0(m)$$

$$q_i(m = 0, t) = 0, \quad q_i(m = \infty, t) = 0, \qquad 1 \leqslant i \leqslant n$$

Here β is the coagulation kernel, H_i the normalized growth rate of species i, S the emission rate (number of particles of mass m per unit time) and L is the first-order rate of removal of particles of mass m. The total particle mass density and the total growth rate are $q = \sum_{i=1}^n q_i$ and $H = \sum_{i=1}^n H_i$ respectively. The numerical integration of this equation remains a challenge, and several current approaches are discussed in [109,111,110].

Algorithms needed for data assimilation with aerosol models are being developed [64,115]. The continuous adjoint equation associated with the general dynamic equation (27) is also an integral partial differential equation

$$\frac{\partial \lambda_i}{\partial t} = - \int_0^\infty \beta(m, m')(m')^{-1} [\lambda_i(m + m', t) - \lambda_i(m, t)] q(m', t) \, dm' + L \lambda_i$$

$$- \int_0^\infty \beta(m', m) m^{-1} \sum_{j=1}^n [\lambda_j(m + m', t) - \lambda_j(m, t)] q_j(m', t) \, dm'$$

$$- \sum_{j=1}^n H_j \lambda_j - m H (\lambda_i)_m - \phi_i, \quad t^0 \leqslant t \leqslant t^F, \quad \lambda_i(m, t^F) = 0, \quad \lambda_i(m = 0, t) = 0 \tag{28}$$
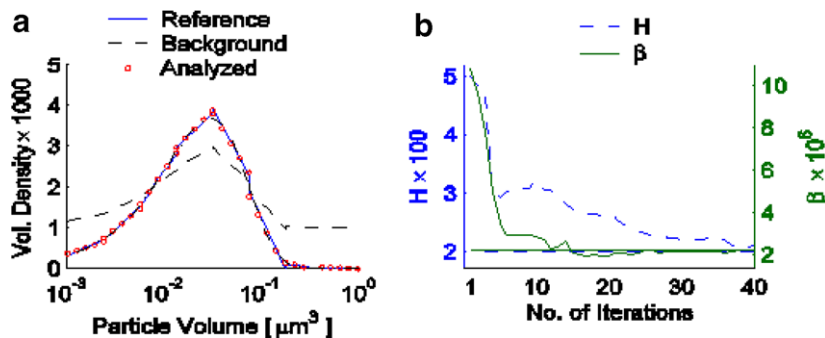
Fig. 23. (a) The reference, perturbed, and recovered initial aerosol densities. The profile recovered through data assimilation (red circles) overlaps the reference profile (blue). (b) The evolution of the recovered model parameter values with the number of optimization iterations during data assimilation. The perturbed values start far from the reference ones (represented by the horizontal line), and they are recovered in about 40 iterations. (For interpretation of the references in colour in this figure legend, the reader is referred to the web version of this article.)

where the forcing term ϕ_i depends on the particular cost function. As an example consider data assimilation with a monomer particle model. Both the initial density and the model parameters (coagulation kernel β and growth rate H) are uncertain. In a twin experiment framework a reference model run (starting from a reference initial distribution and with the reference values of β and H) is used to generate artificial observations (one observation of the evolved density per hour for 48 h of evolution). Then the initial distribution and the model parameters are perturbed, and data assimilation is used to recover the reference values. This is illustrated in Fig. 23. Adjoint approaches for the assimilation of aerosol observations are now emerging in CTMs [63].

8. The road forward

The importance of air quality prediction in the management of our environment continues to grow. The recent developments in atmospheric chemical observations and modeling are also leading to more effective linkages of air pollution issues on different scales from urban to global. It is now recognized that in urban air pollution studies it is important to also consider regional and global contributions, and in global air pollution, the effects of mega-cities and hemispheric transport. In addition, the emergence of chemical weather forecasting as an important activity places greater need on linking pollution detection and prediction capabilities. The close integration of observational data is recognized as essential in weather/climate analysis and forecast activities, and this is accomplished by a mature experience/infrastructure in meteorological data assimilation. Borrowing lessons learned from the evolution of numerical weather prediction (NWP) models, improving air quality predictions through the assimilation of chemical data holds significant promise. As more atmospheric chemical observations become available chemical data assimilation is expected to play an essential role in air quality forecasting, similar to the role it has in NWPs (and may also benefit weather forecasting as well).

Advances in our predictive capabilities will require a better matching of the observational capabilities with chemical weather forecast needs. This will require closer interactions between the observing and the modeling communities. One important activity will be the use of chemical data assimilation systems to help design the observing systems needed to produce better forecasts. We need to rigorously quantify the value-added to a forecast by: adding observations of additional species; extending surface coverage; adding observations above the surface; and adding and enhancing observations from satellites.

Advances will also require a growth in activities related to chemical data assimilation techniques and algorithms. While there is much to build upon from the assimilation expertise and experiences in weather prediction, there are significant differences and challenges related to chemical weather. As we have illustrated in this paper 4D-Var and EnKF are powerful techniques, and there are exciting possibilities in combining their strengths in hybrid data assimilation methods. However, there is relatively little experience in applying modern data assimilation techniques to real atmospheric chemistry problems, and much work needs to be done before their true impact on air quality prediction is felt.

Furthermore, feedbacks between the meteorological and air quality components – which have mostly been studied as separate systems – are also critical to improving AQ forecasts. Many challenging and important questions remain to be addressed, including: What is the relationship between mixing depth heights and near surface concentrations? What is the role of ambient aerosols in influencing the surface energy budgets and in altering the moisture fields via cloud interactions? How do these feedbacks impact weather and AQ forecasts? And to what extent will the assimilation of chemical data lead to improvements in weather forecasting? Sensitivity analysis studies are needed to quantify these feedbacks, which in turn can help prioritize future research efforts. Addressing these issues will require a closer integration of meteorological and air quality models, and ultimately the evolution to tightly coupled combined meteorological and air quality forecasting and data assimilation systems. These aspects are being explored in projects such as the European Union Global and regional Earth-system (Atmosphere) Monitoring using Satellite and in situ data (GEMS) [1] project. The integration of enhanced observing systems with modeling tools for use in air quality and climate change is a priority area within the Global Earth Observing System of Systems (GEOSS) [75] and the Integrated Global Atmospheric Chemistry Observations (IGACO) [2] frameworks. IGACO is a focused strategy for bringing together ground-based, aircraft and satellite observations using atmospheric forecast models that assimilate not only meteorological observations but also chemical constituents.

Finally, the requirements to use CTMs for urban to global scale applications, to couple chemistry with weather and climate, and to incorporate data assimilation, place even more demands for computational efficiency and accuracy. The growing importance of chemical weather forecasting to society should help stimulate significant advances in the field over the next decade.

Acknowledgments

References

[1] Gems description of work: global & regional earth-system monitoring using satellite and in situ data, September 2004, Call Identifier FP6-2003-SPACE-1; OJ Reference OJ C303 of 13.12.2003.
[2] The changing atmosphere: an integrated global atmospheric chemistry observation theme for the IGOS partnership, September 2004, Report GAW No.159 (WMO TD No.1235).
[3] S. Akella, I.M. Navon, A comparative study of the performance of high resolution advection schemes in the context of data assimilation, Int. J. Numer. Methods Fluids 51 (7) (2006) 719–748.
[4] J.L. Anderson, An ensemble adjustment Kalman filter for data assimilation, Mon. Weather Rev. 129 (12) (2001) 2884–2903.
[5] J.L. Anderson, S.L. Anderson, A monte carlo implementation of the nonlinear filtering problem to produce ensemble assimilations and forecasts, Mon. Weather Rev. 127 (12) (1999) 2741–2758.
[6] A.F. Arellano, P.S. Kasibhatla, L. Giglio, G.R. van der Werf, J.T. Randerson, Top-down estimates of global CO sources using MOPITT measurements, Geophys. Res. Lett. 31 (12) (2004). Art No. L01104.
[7] T.V. Babovic, D.R. Fuhrman, Data assimilation of local model error forecasts in a deterministic model, Int. J. Numer. Methods Fluids 39 (10) (2002) 887–918.
[8] T.S. Bates, T.L. Anderson, T. Baynard, T. Bond, O. Boucher, G. Carmichael, A. Clarke, C. Erlick, H. Guo, L. Horowitz, S. Howell, S. Kulkarni, H. Maring, A. McComiskey, A. Middlebrook, K. Noone, C.D. O'Dowd, J. Ogren, J. Penner, P.K. Quinn, A.R. Ravishankara, D.L. Savoie, S.E. Schwartz, Y. Shinozuka, Y. Tang, R.J. Weber, Y. Wu, Aerosol direct radiative effects over the northwest Atlantic, northwest pacific, and north Indian oceans: estimates based on in situ chemical and optical measurements and chemical transport modeling, Atmos. Chem. Phys. 6 (2006) 1657–1732.
[9] T. Bergot, Influence of the assimilation scheme on the efficiency of adaptive observations, Quart. J. Roy. Meteor. Soc. Part B 127 (572) (2001) 635–660.
[10] T. Bergot, A. Doerenbecher, A study on the optimization of the deployment of targeted observations using adjoint-based methods, Quart. J. Roy. Meteor. Soc. Part A 128 (583) (2002) 1689–1712.
[11] C.H. Bishop, B.J. Etherton, S.J. Majumdar, Adaptive sampling with the ensemble transform Kalman filter. part I: theoretical aspects, Mon. Weather Rev. 129 (3) (2001) 420–436.
[12] M. Bocquet, Reconstruction of an atmospheric tracer source using the principle of maximum entropy. I: theory, Quart. J. Roy. Meteor. Soc. Part B 131 (610) (2005) 2191–2208.
[13] M. Bocquet, Reconstruction of an atmospheric tracer source using the principle of maximum entropy. II: applications, Quart. J. Roy. Meteor. Soc. Part B 131 (610) (2005) 2209–2223.

[14] R. Buizza, A. Montani, Targeting observations using singular vectors, J. Atmos. Sci. 56 (17) (1999) 2965–2985.

[15] R. Buizza, T.N. Palmer, The singular-vector structure of the atmospheric global circulation, J. Atmos. Sci. 52 (9) (1995) 1434–1456.

[16] G. Burgers, P.J. van Leeuwen, G. Evensen, Analysis scheme in the ensemble Kalman filter, Mon. Weather Rev. 126 (6) (1998) 1719–1724.

[17] R.H. Byrd, P.H. Lu, J. Nocedal, C.Y. Zhu, A limited memory algorithm for bound constrained optimization, SIAM J. Sci. Comput. 16 (5) (1995) 1190–1208.

[18] D.G. Cacuci, Sensitivity theory for non-linear systems. 1. Non-linear functional-analysis approach, J. Math. Phys. 22 (12) (1981) 2794–2802.

[19] D.G. Cacuci, Sensitivity theory for non-linear systems. 2. Extensions to additional classes of responses, J. Math. Phys. 22 (12) (1981) 2803–2812.

[20] D.G. Cacuci, Sensitivity and Uncertainty Analysis, Chapman & Hall/CRC, Boca Raton, FL, 2003.

[21] G.R. Carmichael, D.N. Daescu, A. Sandu, T. Chai, Computational aspects of chemical data assimilation into atmospheric models, in: Computational Science – ICCS 2003, PT. IV in Lecture Notes in Computer Science, Springer-Verlag, Berlin, 2003, pp. 269–278.

[22] G.R. Carmichael, Y. Tang, G. Kurata, I. Uno, D. Streets, J.H. Woo, H. Huang, J. Yienger, B. Lefer, R. Shetter, D. Blake, E. Atlas, A. Fried, E. Apel, F. Eisele, C. Cantrell, M. Avery, J. Barrick, G. Sachse, W. Brune, S. Sandholm, Y. Kondo, H. Singh, R. Talbot, A. Bandy, D. Thorton, A. Clarke, B. Heikes, Regional-scale chemical transport modeling in support of the analysis of observations obtained during the TRACE-P experiment, J. Geophys. Res. 108 (D21) (2003). Art. No. 8823.

[23] W.P.L. Carter, Documentation of the SAPRC-99 chemical mechanism for VOC reactivity assessment, Technical Report 92-329, California Air Resources Board Contract, May 2000.

[24] T. Chai, G.R. Carmichael, D.N. Daescu, A. Sandu, Analysis of TRACE-P observations using a four-dimensional variational data assimilation technique, in: Preprint of 84th American Meteorological Society Annual Meeting, Seattle, WA, USA, 11–15 January 2004.

[25] T. Chai, G.R. Carmichael, A. Sandu, M. Hardesty, P. Pilewskie, S. Whitlow, E.V. Browell, M.A. Avery, V. Thouret, P. Nedelec, J.T. Merrill, A.M. Thompson, Four dimensional data assimilation experiments with ICARTT (International Consortium for Atmospheric Research on Transport and Transformation) ozone measurements, J. Geophys. Res., in press, doi:10.1029/2006JD007763.

[26] T. Chai, G.R. Carmichael, A. Sandu, Y.H. Tang, D.N. Daescu, Chemical data assimilation of transport and chemical evolution over the pacific (TRACE-P) aircraft measurements, J. Geophys. Res. 111 (D02301) (2006), doi:10.1029/2005JD005883.

[27] D.P. Chock, G.R. Carmichael (Eds.), Atmospheric Modeling, Springer, 2002.

[28] S.E. Cohn, An introduction to estimation theory, J. Meteorol. Soc. Jpn. 75 (1B) (1997) 257–288.

[29] W.D. Collins, P.J. Rasch, B.E. Eaton, B.V. Khattatov, J.F. Lamarque, C.S. Zender, Simulating aerosols using a chemical transport model with assimilation of satellite aerosol retrievals: methodology for INDOEX, J. Geophys. Res. 106 (D7) (2001) 7313–7336.

[30] E.M. Constantinescu, A. Sandu, On adaptive mesh refinement for atmospheric pollution models, in: Computational Science – ICCS 2005, Pt 2, Lecture Notes in Computer Science, vol. 3515, Springer-Verlag, Berlin, 2005, pp. 798–805.

[31] E.M. Constantinescu, A. Sandu, T. Chai, G.R. Carmichael, Autoregressive models of background errors for chemical data assimilation, J. Geophys. Res., in press.

[32] E.M. Constantinescu, A. Sandu, T. Chai, G.R. Carmichael, Ensemble-based chemical data assimilation. I: General approach, Quart. J. Roy. Meteor. Soc., in press.

[33] E.M. Constantinescu, A. Sandu, T. Chai, G.R. Carmichael, Ensemble-based chemical data assimilation. II: Covariance localization, Quart. J. Roy. Meteor. Soc., in press.

[34] M. Corazza, E. Kalnay, D. Patil, Use of the breeding technique to estimate the shape of the analysis "errors of the day", Nonlinear Process. Geophys. 10 (2002) 233–243.

[35] P. Courtier, J.N. Thepaut, A. Hollingsworth, A strategy for operational implementation of 4D-Var, using an incremental approach, Quart. J. Roy. Meteor. Soc. 120 (519) (1994) 1367–1387.

[36] W.F. Dabberdt, M.A. Carroll, D. Baumgardner, G. Carmichael, R. Cohen, T. Dye, J. Ellis, G. Grell, S. Grimmond, S. Hanna, J. Irwin, B. Lamb, S. Madronich, J. McQueen, J. Meagher, T. Odman, J. Pleim, H.P. Schmid, D.L. Westphal, Meteorological research needs for improved air quality forecasting – Report of the 11th prospectus development team of the US weather research program, Bull. Amer. Meteorol. Soc. 85 (4) (2004) 563.

[37] D.N. Daescu, G.R. Carmichael, An adjoint sensitivity method for the adaptive location of the observations in air quality modeling, J. Atmos. Sci. 60 (2) (2003) 434–450.

[38] D.N. Daescu, I.M. Navon, A dual-weighted approach to order reduction in 4D-Var data assimilation, Mon. Weather Rev., in review.

[39] D.N. Daescu, I.M. Navon, Efficiency of a pod-based reduced second-order adjoint model in 4D-Var data assimilation, Int. J. Numer. Methods Fluids. 53 (6) (2007) 985–1004.

[40] D.N. Daescu, I.M. Navon, Adaptive observations in the context of 4D-Var data assimilation, Meteorol. Atmos. Phys. 85 (4) (2004) 205–226.

[41] R. Daley, Estimating model-error covariances for application to atmospheric data assimilation, Mon. Weather Rev. 120 (8) (1992) 1735–1746.

[42] V. Damian, A. Sandu, M. Damian, F. Potra, G.R. Carmichael, The kinetic preprocessor KPP – a software environment for solving chemical kinetics, Comput. Chem. Eng. 26 (11) (2002) 1567–1579.

[43] L. Delle Monache, R.B. Stull, An ensemble air-quality forecast over western Europe during an ozone episode, Atmos. Environ. 37 (25) (2003) 3469–3474.

[44] J. Derber, F. Bouttier, A reformulation of the background error covariance in the ECMWF global data assimilation system, Tellus Series – Dyn. Meteorol. Oceanogr. 51 (2) (1999) 195–221.

[45] A.M. Dunker, Decoupled direct method for calculating sensitivity coefficients in chemical kinetics, J. Chem. Phys. 81 (1984) 2385–2393.

[46] H. Elbern, H. Schmidt, A 4D-Var chemistry data assimilation scheme for Eulerian chemistry transport modeling, J. Geophys. Res. 104 (D15) (1999) 18583–18598.

[47] H. Elbern, H. Schmidt, Ozone episode analysis by four-dimensional variational chemistry data assimilation, J. Geophys. Res. 106 (D4) (2001) 3569–3590.

[48] H. Elbern, H. Schmidt, A. Ebel, Implementation of a parallel 4D-Var chemistry data assimilation scheme, Environ. Manage. Health 10 (1999) 236–244.

[49] H. Elbern, H. Schmidt, O. Talagrand, A. Ebel, 4D-variational data assimilation with an adjoint air quality model for emission analysis, Environ. Model. Software 15 (2000) 539–548.

[50] G. Evensen, Using the extended Kalman filter with a multilayer quasi-geostrophic ocean model, J. Geophys. Res. 97 (C11) (1992) 17905–17924.

[51] G. Evensen, Open boundary-conditions for the extended Kalman filter with a quasi-geostrophic ocean model, J. Geophys. Res. 98 (C9) (1993) 16529–16546.

[52] G. Evensen, Sequential data assimilation with a nonlinear quasi-geostrophic model using monte-carlo methods to forecast error statistics, J. Geophys. Res. 99 (C5) (1994) 10143–10162.

[53] G. Evensen, The ensemble Kalman filter: theoretical formulation and practical implementation, Ocean Dyn. 53 (4) (2003) 343–367.

[54] G. Evensen, P.J. van Leeuwen, An ensemble Kalman smoother for nonlinear dynamics, Mon. Weather Rev. 128 (6) (2000) 1852–1867.

[55] M. Fisher, Background error covariance modelling, in: Proceedings of the ECMWF Workshop on Recent Developments in Data Assimilation for Atmosphere and Ocean, Reading, UK, 8–12 September 2003.

[56] M. Fisher, D.J. Lary, Lagrangian 4-dimensional variational data assimilation of chemical-species, Quart. J. Roy. Meteor. Soc. Part A 121 (527) (1995) 1681–1704.

[57] R. Gelaro, R. Buizza, T.N. Palmer, E. Klinker, Sensitivity analysis of forecast errors and the construction of optimal perturbations using singular vectors, J. Atmos. Sci. 55 (6) (1998) 1012–1037.

[58] G.A. Grell, S.E. Peckham, R. Schmitz, S.A. McKeen, G. Frost, W.C. Skamarock, B. Eder, G. Petron, C. Granier, B. Khattatov, V. Yudin, J.F. Lamarque, L. Emmons, J. Gille, D.P. Edwards, Fully coupled "online" chemistry within the WRF model, Geophys. Res. Lett. 39 (37) (2005) 6957–6975.

[59] A. Hakami, D.K. Henze, J.H. Seinfeld, T. Chai, Y. Tang, G.R. Carmichael, A. Sandu, Adjoint inverse modeling of black carbon during the Asian pacific regional aerosol characterization experiment, J. Geophys. Res. 110 (D14) (2005). Art. No. D14301.

[60] T.M. Hamill, J.S. Whitaker, C. Snyder, Distance-dependent filtering of background error covariance estimates in an ensemble Kalman filter, Mon. Weather Rev. 129 (11) (2001) 2776–2790.

[61] J.A. Hansen, Accounting for model error in ensemble-based state estimation and forecasting, Mon. Weather Rev. 130 (10) (2002) 2373–2391.

[62] J.A. Hansen, L.A. Smith, Probabilistic noise reduction, Tellus Series – Dyn. Meteorol. Oceanogr. 53 (5) (2001) 585–598.

[63] D.K. Henze, J.H. Seinfeld, Development of the adjoint of geos-chem, Atmos. Chem. Phys. Discuss. 6 (2006) 10591–10648.

[64] D.K. Henze, J.H. Seinfeld, W. Liao, A. Sandu, G.R. Carmichael, Inverse modeling of aerosol dynamics: condensational growth, J. Geophys. Res. 109 (D14) (2004) D14201, doi:10.1029/2004JD004593.

[65] L.M. Herschel, P.L. Houtekamer, Ensemble size, balance, and model-error representation in ENKF, Mon. Weather Rev. 125 (2002) 2416–2426.

[66] P.L. Houtekamer, L. Lefaivre, Using ensemble forecasts for model validation, Mon. Weather Rev. 125 (10) (1997) 2416–2426.

[67] P.L. Houtekamer, H.L. Mitchell, Data assimilation using an ensemble Kalman filter technique, Mon. Weather Rev. 126 (3) (1998) 796–811.

[68] P.L. Houtekamer, H.L. Mitchell, A sequential ensemble Kalman filter for atmospheric data assimilation, Mon. Weather Rev. 129 (1) (2001) 123–137.

[69] B.R. Hunt, E. Kalnay, E.J. Kostelich, E. Ott, D.J. Patil, T. Sauer, I. Szunyogh, J.A. Yorke, A.V. Zimin, Four-dimensional ensemble Kalman filtering, Tellus Series – Dyn. Meteorol. Oceanogr. 56 (4) (2004) 273–277.

[70] D.J. Jacob, J.H. Crawford, M.M. Kleb, V.S. Connors, R.J. Bendura, J.L. Raper, G.W. Sachse, J.C. Gille, L. Emmons, C.L. Heald, Transport and chemical evolution over the pacific (TRACE-P) aircraft mission: design, execution, and first results, J. Geophys. Res. 108 (D20) (2003) 1–19.

[71] M.E. Jenkin, S.M. Saunders, M.J. Pilling, The tropospheric degradation of volatile organic compounds: a protocol for mechanism development, Atmos. Environ. 31 (1997) 81–104.

[72] R.E. Kalman, A new approach to linear filtering and prediction problems, Trans. ASME, Ser. D: J. Basic Eng. 82 (1960) 35–45.

[73] E. Kalnay, Atmospheric Modeling, Data Assimilation, and Predictability, Cambridge University Press, Cambridge, UK; New York, 2003.

[74] C.M. Kiley, H.E. Fuelberg, P.I. Palmer, D.J. Allen, G.R. Carmichael, D.J. Jacob, C. Mari, R.B. Pierce, K.E. Pickering, Y.H. Tang, O. Wild, T.D. Fairlie, J.A. Logan, G.W. Sachse, T.K. Shaack, D.G. Streets, An intercomparison and evaluation of aircraft-derived and simulated CO from seven chemical transport models during the TRACE-P experiment, J. Geophys. Res. 108 (D21) (2003). Art. No. 8819.

[75] V.N. Krutikov, V.I. Sapritsky, B.B. Khlevnoy, B.E. Lisiansky, S.P. Morozova, S.A. Ogarev, A.S. Panfilov, M.K. Sakharov, M.L. Samoylov, G. Bingham, T. Humpherys, A. Thurgood, V.E. Privalsky, The global earth observation system of systems (GEOSS) and metrological support for measuring radiometric properties of objects of observations, Metrologia 43 (2) (2006) S94–S97.

[76] E. Kucukkaraca, M. Fisher, Use of analysis ensembles in estimating flow-dependent background error variances, ECMWF technical memorandum 492, The European Centre for Medium-Range Weather Forecasts, January 2006.

[77] R.H. Langland, A.L. Baker, Estimation of observation impact using the NRL atmospheric variational data assimilation adjoint system, Tellus Series – Dyn. Meteorol. Oceanogr. 56 (3) (2004) 189–201.

[78] R.H. Langland, Z. Toth, R. Gelaro, I. Szunyogh, M.A. Shapiro, S.J. Majumdar, R.E. Morss, G.D. Rohaly, C. Velden, N. Bond, C.H. Bishop, The north Pacific experiment (NORPEX-98): targeted observations for improved North American weather forecasts, Bull. Amer. Meteorol. Soc. 80 (7) (1999) 1363–1384.

[79] M.G. Lawrence, P.J. Rasch, R. von Kuhlmann, J. Williams, H. Fischer, M. de Reus, J. Lelieveld, P.J. Crutzen, M. Schultz, P. Stier, H. Huntrieser, J. Heland, A. Stohl, C. Forster, H. Elbern, H. Jakobs, R.R. Dickerson, Global chemical weather forecasts for field campaign planning: predictions and observations of large-scale features during minos, contrace, and indoex, Atmos. Chem. Phys. 3 (2003) 267–289.

[80] F.-X. Le Dimet, I.M. Navon, D.N. Daescu, Second-order information in data assimilation, Mon. Weather Rev. 130 (3) (2002) 629–648.

[81] F.X. Le Dimet, O. Talagrand, Variational algorithms for analysis and assimilation of meteorological observations – theoretical aspects, Tellus Series – Dyn. Meteorol. Oceanogr. 38 (2) (1986) 97–110.

[82] A.M. Lee, G.D. Carver, M.P. Chipperfield, J.A. Pyle, Three-dimensional chemical forecasting: a methodology, J. Geophys. Res. 102 (D3) (1997) 3905–3919.

[83] M. Leutbecher, A reduced rank estimate of forecast error variance changes due to intermittent modifications of the observing network, J. Atmos. Sci. 60 (5) (2003) 729–742.

[84] W.Y. Liao, A. Sandu, Total energy singular vectors for atmospheric chemical transport models, in: Computational Science – ICCS 2005, no. II in Lecture Notes in Computer Science, vol. 3515, Springer-Verlag, Berlin, 2005, pp. 806–813.

[85] W.Y. Liao, A. Sandu, G.R. Carmichael, T. Chai, Singular vector analysis for atmospheric chemical transport models, Mon. Weather Rev., in press.

[86] Z. Liu, A. Sandu, Analysis of discrete adjoints for upwind numerical schemes, in: Computational Science – ICCS 2005, Pt 2, Lecture Notes in Computer Science, vol. 3515, Springer-Verlag, Berlin, 2005, pp. 829–836.

[87] A.C. Lorenc, Analysis-methods for numerical weather prediction, Quart. J. Roy. Meteor. Soc. 112 (474) (1986) 1177–1194.

[88] E.N. Lorenz, K.A. Emanuel, Optimal sites for supplementary weather observations: simulation with a small model, J. Atmos. Sci. 55 (3) (1998) 399–414.

[89] T. Løvås, E. Mastorakos, D.A. Goussis, Reduction of the RACM scheme using computational singular perturbation analysis, J. Geophys. Res. 111 (D13302) (2006), doi:10.1029/2005JD006743.

[90] S.J. Majumdar, C.H. Bishop, R. Buizza, R. Gelaro, A comparison of ensemble-transform Kalman-filter targeting guidance with ECMWF and NRL total-energy singular-vector guidance, Quart. J. Roy. Meteor. Soc. 128 (585) (2002) 2527–2549.

[91] V. Mallet, B. Sportisse, Ensemble-based air quality forecasts: a multimodel approach applied to ozone, J. Geophys. Res. 111 (D18302) (2006), doi:10.1029/2005JD006675.

[92] G.I. Marchuk, Adjoint Equations and Analysis of Complex Systems, Kluwer Academic Publishers, Dordrecht, Boston, 1995.

[93] S.A. McKeen, S.H. Chung, J. Wilczak, G. Grell, I. Djalalova, S. Peckham, W. Gong, V. Bouchet, R. Moffet, Y. Tang, G.R. Carmichael, R. Mathur, S. Yu, The evaluation of several pm2.5 forecast models using data collected during the ICARTT/NEAQS 2004 field study, J. Geophys. Res. 112 (2007) Art. No. D10S20, doi:10.1029/2006JD007608.

[94] S.A. McKeen, J. Wilczak, G. Grell, I. Djalalova, S. Peckham, E. Hsie, W. Gong, V. Bouchet, S. Menard, R. Moffet, J. McHenry, J. McQueen, Y. Tang, G.R. Carmichael, M. Pagowski, A. Chan, T. Dye, G. Frost, P. Lee, R. Mathur, Assessment of an ensemble of seven real-time ozone forecasts over eastern North America during the summer of 2004, J. Geophys. Res. 110 (D21) (2005) Art. No. D21307.

[95] Z. Meng, D. Dabdub, J.H. Seinfeld, Size-resolved and chemically resolved model of atmospheric aerosol dynamics, J. Geophys. Res. 103 (D3) (1998) 3419–3436.

[96] L. Menut, R. Vautard, M. Beekmann, C. Honore, Sensitivity of photochemical pollution using the adjoint of a simplified chemistry-transport model, J. Geophys. Res. 105 (D12) (2000) 15379–15402.

[97] P. Miehe, A. Sandu, G.R. Carmichael, Y.H. Tang, D. Daescu, A communication library for the parallelization of air quality models on structured grids, Atmos. Environ. 36 (24) (2002) 3917–3930.

[98] R.E. Morss, K.A. Emanuel, C. Snyder, Idealized adaptive observation strategies for improving numerical weather prediction, J. Atmos. Sci. 58 (2) (2001) 210–232.

[99] I.M. Navon, Practical and theoretical aspects of adjoint parameter estimation and identifiability in meteorology and oceanography, Dyn. Atmosph. Oceans 27 (1–4) (1998) 55–79.

[100] G. Pétron, C. Granier, B. Khattatov, V. Yudin, J.F. Lamarque, L. Emmons, J. Gille, D.P. Edwards, Monthly CO surface sources inventory based on the 2000–2001 MOPITT satellite data, Geophys. Res. Lett. 31 (21) (2004). Art. No. L21107.

[101] M. Pagowski, G.A. Grell, S.A. McKeen, D. Dèvènyi, J.M. Wilczak, V. Bouchet, W. Gong, J. McHenry, S. Peckham, J. McQueen, R. Moffet, Y. Tang, A simple method to improve ensemble-based ozone forecasts, Geophys. Res. Lett. 32 (L07814) (2005), doi:10.1029/2004GL022305.

[102] P.I. Palmer, D.J. Jacob, D.B.A. Jones, C.L. Heald, R.M. Yantosca, J.A. Logan, G.W. Sachse, D.G. Streets, Inverting for emissions of carbon monoxide from Asia using aircraft observations over the western Pacific, J. Geophys. Res. 108 (D21) (2003). Art. No. 8828.

[103] L. Pan, T. Chai, G.R. Carmichael, Y. Tang, D. Streets, J. Woo, H.R. Friedli, L.F. Radke, Top-down estimate of mercury emissions in China using four-dimensional variational data assimilation (4D-Var), Atmos. Environ. 41 (13) (2007) 2804–2819.
[104] D.F. Parrish, J.C. Derber, The national-meteorological-centers spectral statistical-interpolation analysis system, Mon. Weather Rev. 120 (8) (1992) 1747–1763.
[105] D.T. Pham, Stochastic methods for sequential data assimilation in strongly nonlinear systems, Mon. Weather Rev. 129 (5) (2001) 1194–1207.
[106] E. Rabier, H. Jarvinen, E. Klinker, J.F. Mahfouf, A. Simmons, The ECMWF operational implementation of four-dimensional variational assimilation. I: Experimental results with simplified physics, Quart. J. Roy. Meteor. Soc. 126 (564) (2000) 1143–1170.
[107] F. Rabier, E. Klinker, P. Courtier, A. Hollingsworth, Sensitivity of forecast errors to initial conditions, Quart. J. Roy. Meteor. Soc. 122 (529) (1996) 121–150.
[108] P.J. Rasch, W.D. Collins, B.E. Eaton, Understanding the Indian ocean experiment (INDOEX) aerosol distributions with an aerosol assimilation, J. Geophys. Res. 106 (D7) (2001) 7337–7355.
[109] A. Sandu, A newton-cotes quadrature approach for solving the aerosol coagulation equation, Atmos. Environ. 36 (3) (2002) 583–589.
[110] A. Sandu, Piecewise polynomial solutions of aerosol dynamic equation, Aerosol Sci. Technol. 40 (4) (2006) 261–273.
[111] A. Sandu, C. Borden, A framework for the numerical treatment of aerosol dynamics, Appl. Numer. Math. 45 (4) (2003) 475–497.
[112] A. Sandu, E.M. Constantinescu, W.Y. Liao, G.R. Carmichael, T.F. Chai, J.H. Seinfeld, D. Daescu, Ensemble-based data assimilation for atmospheric chemical transport models, in: Computational Science – ICCS 2005, Pt 2, Lecture Notes in Computer Science, vol. 3515, Springer-Verlag, Berlin, 2005, pp. 648–655.
[113] A. Sandu, D.N. Daescu, G.R. Carmichael, Direct and adjoint sensitivity analysis of chemical kinetic systems with KPP: Part I – theory and software tools, Atmos. Environ. 37 (36) (2003) 5083–5096.
[114] A. Sandu, D.N. Daescu, G.R. Carmichael, T.F. Chai, Adjoint sensitivity analysis of regional air quality models, J. Comput. Phys. 204 (1) (2005) 222–252.
[115] A. Sandu, W. Liao, G.R. Carmichael, D.K. Henze, J.H. Seinfeld, Inverse modeling of aerosol dynamics using adjoints: theoretical and numerical considerations, Aerosol Sci. Technol. 39 (8) (2005) 677–694, doi:10.1080/02786820500182289.
[116] A. Sandu, R. Sander, Technical note: simulating chemical systems in fortran90 and matlab with the kinetic preprocessor KPP-2.1, Atmos. Chem. Phys. 6 (2006) 187–195.
[117] S. Schubert, Y.H. Chang, An objective method for inferring sources of model error, Mon. Weather Rev. 124 (2) (1996) 325–340.
[118] H.B. Singh, W.H. Brune, J.H. Crawford, D.J. Jacob, P.B. Russell, Overview of the summer 2004 Intercontinental Chemical Transport Experiment-North America (INTEX-A), J. Geophys. Res. 111 (D24) (2006) D24S01, doi:10.1029/2006JD007905.
[119] D.G. Streets, Q. Zhang, L. Wang, K. He, J. Hao, Y. Wu, Y. Tang, G. Carmichael, Revisting China's CO emissions after transport chemical evolution over the pacific (TRACE-P): synthesis of inventories atmospheric modeling and observations, J. Geophys. Res. 111 (D14) (2006). Art No. D14306.
[120] O. Talagrand, P. Courtier, Variational assimilation of meteorological observations with the adjoint vorticity equation. 1. Theory, Quart. J. Roy. Meteor. Soc. 113 (478) (1987) 1311–1328.
[121] Y.H. Tang, G.R. Carmichael, N. Thongboonchoo, T. Chai, L.W. Horowitz, R.B. Pierce, J.A. Al-Saadi, G. Pfister, M. Vukovich, M.A. Avery, G.W. Sachse, T.B. Ryerson, J.S. Holloway, E.L. Atlas, F.M. Flocke, R.J. Weber, L.G. Huey, J.E. Dibb, D.G. Streets, W.H. Brune, The influence of lateral and top boundary conditions on regional air quality prediction: a multi-scale study coupling regional and global chemical transport models, J. Geophys. Res., in press, doi:10.1029/2006JD007515.
[122] J. Thuburn, T.W.N. Haine, Adjoints of nonoscillatory advection schemes, J. Comput. Phys. 171 (2) (2001) 616–631.
[123] T. Vukicevic, M. Steyskal, M. Hecht, Properties of advection algorithms in the context of variational data assimilation, Mon. Weather Rev. 129 (5) (2001) 1221–1231.
[124] A. Weaver, P. Courtier, Correlation modelling on the sphere using a generalized diffusion equation, Quart. J. Roy. Meteor. Soc. 127 (575) (2001) 1815–1846.
[125] L.E. Whitehouse, A.S. Tomlin, M.J. Pilling, Systematic reduction of complex tropospheric chemical mechanisms, Part II: lumping using a time-scale based approach, Atmos. Chem. Phys. 4 (7) (2004) 2057–2081.
[126] J. Wilczak, S. McKeen, I. Djalalova, G. Grell, S. Peckham, W. Gong, V. Bouchet, R. Moffet, J. McHenry, J. McQueen, P. Lee, Y. Tang, G.R. Carmichael, Bias-corrected ensemble and probabilistic forecasts of surface ozone over eastern North America during the summer of 2004, J. Geophys. Res. 111 (2006) D23S28, doi:10.1029/2006JD007598.
[127] C. Zhu, R.H. Byrd, J. Nocedal, L-BFGS-B–fortran routines for large scale bound constrained optimization, ACM Trans. Math. Software 23 (4) (1997) 550–560.
[128] Z. Zlatev (Ed.), Computer Treatment of Large Air Pollution Models, Kluwer Academic Publishers, 1995.